ACS NANO

www.acsnano.org

Bioengineered Bacteriophage-Like Nanoparticles as RNAi Therapeutics to Enhance Radiotherapy against Glioblastomas

Hao-Han Pang, Chiung-Yin Huang, Pin-Yuan Chen, Nan-Si Li, Ying-Pei Hsu, Jan-Kai Wu, Hsiu-Fang Fan, Kuo-Chen Wei,* and Hung-Wei Yang*

Cite This: *ACS Nano* 2023, 17, 10407−10422

Read Online

ACCESS | Metrics & More | Article Recommendations | Supporting Information

ABSTRACT: Since glioblastomas (GBMs) are radioresistant malignancies and most GBM recurrences occur in radiotherapy, increasing the effectiveness of radiotherapy by gene-silencing has recently attracted attention. However, the difficulty in precisely tuning the composition and RNA loading in nanoparticles leads to batch-to-batch variations of the RNA therapeutics, thus significantly restricting their clinical translation. Here, we bioengineer bacteriophage Qβ particles with a designed broccoli light-up three-way junction (b-3WJ) RNA scaffold (contains two siRNA/miRNA sequences and one light-up aptamer) packaging for the silencing of genes in radioresistant GBM cells. The *in vitro* results demonstrate that the cleavage of *de novo* designed b-3WJ RNA by Dicer enzyme can be easily monitored in real-time using fluorescence microscopy, and the TrQβ@b-3WJ$^{siEGFR}_{Let\text{-}7g}$ successfully knocks down EGFR and IKKα simultaneously and thereby inactivates NF-κB signaling to inhibit DNA repair. Delivery of TrQβ@b-3WJ$^{siEGFR}_{Let\text{-}7g}$ through convection-enhanced delivery (CED) infusion followed by 2Gy X-ray irradiation demonstrated that the median survival was prolonged to over 60 days compared with the 2Gy X-ray irradiated group (median survival: 31 days). Altogether, the results of this study could be critical for the design of RNAi-based genetic therapeutics, and CED infusion serves as a powerful delivery system for promoting radiotherapy against GBMs without evidence of systemic toxicity.

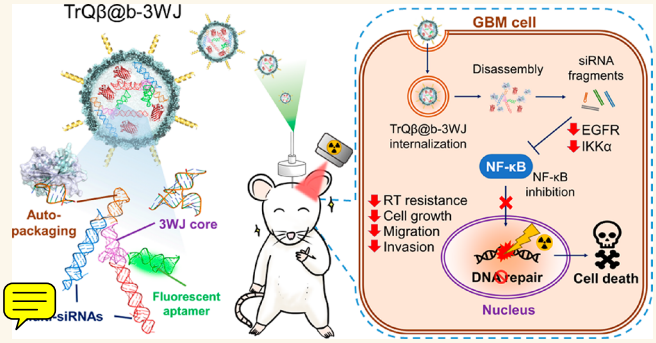

KEYWORDS: *3WJ RNAs, gene silencing, virus-like particles (VLPs), RNAi therapeutics, radioresistance, brain tumors*

INTRODUCTION

Glioblastomas (GBMs) are primary brain tumors characterized by aggressive growth and rapid recurrence.[1] Newly diagnosed GBM patients who receive debulking surgery and adjuvant radiotherapy combined with Temozolomide (TMZ) chemotherapy, both treatments inducing DNA damage,[2] have an average survival of 14.6 months.[3] Despite aggressive treatment, patients always succumb to recurrence-related death, especially radiation resistance. Radiation resistance in GBMs is generally attributed to the hypoxic tumor microenvironment, which creates insufficient oxygen supply thereby rendering tumors highly resistant to radiation-induced killing through rapid DNA repair.[4,5] Previous studies have also suggested that CD133-positive tumor cells represent the cellular population that confers glioma radiation resistance and could be the source of tumor recurrence after radiation.[6,7] In addition, chemotherapy and radiation therapy-induced stress can lead to dedifferentiation of tumor cells to a glioma stem cells (GSCs)-like state, and the GSCs have been shown to promote tumor recurrence.[8]

GBMs respond to DNA damage induced by ionizing radiation (IR) and TMZ treatment through increased expression of DNA repair enzymes, including the proteins O-6-methylguanine-DNA methyltransferase (MGMT) and poly-(ADP-ribose) polymerase 1 (PARP-1).[9] Thus, there is an urgent need to quickly identify the molecular basis of therapy resistance in the primary tumors of GBM patients and develop strategies to abrogate the repair by effectively knocking down the target genes in primary and/or recurrent tumors. RNA

Received: February 6, 2023
Accepted: April 19, 2023
Published: April 25, 2023

https://doi.org/10.1021/acsnano.3c01102
ACS Nano 2023, 17, 10407−10422

Scheme 1. Schematic Illustration of the Effective Tumor Radiotherapy with Enhancing RNAi Penetration and Inhibiting DNA Repair in GBMs by TrQβ@b-3WJ$^{siEGFR}_{Let\text{-}7g}$ Using CED Infusion

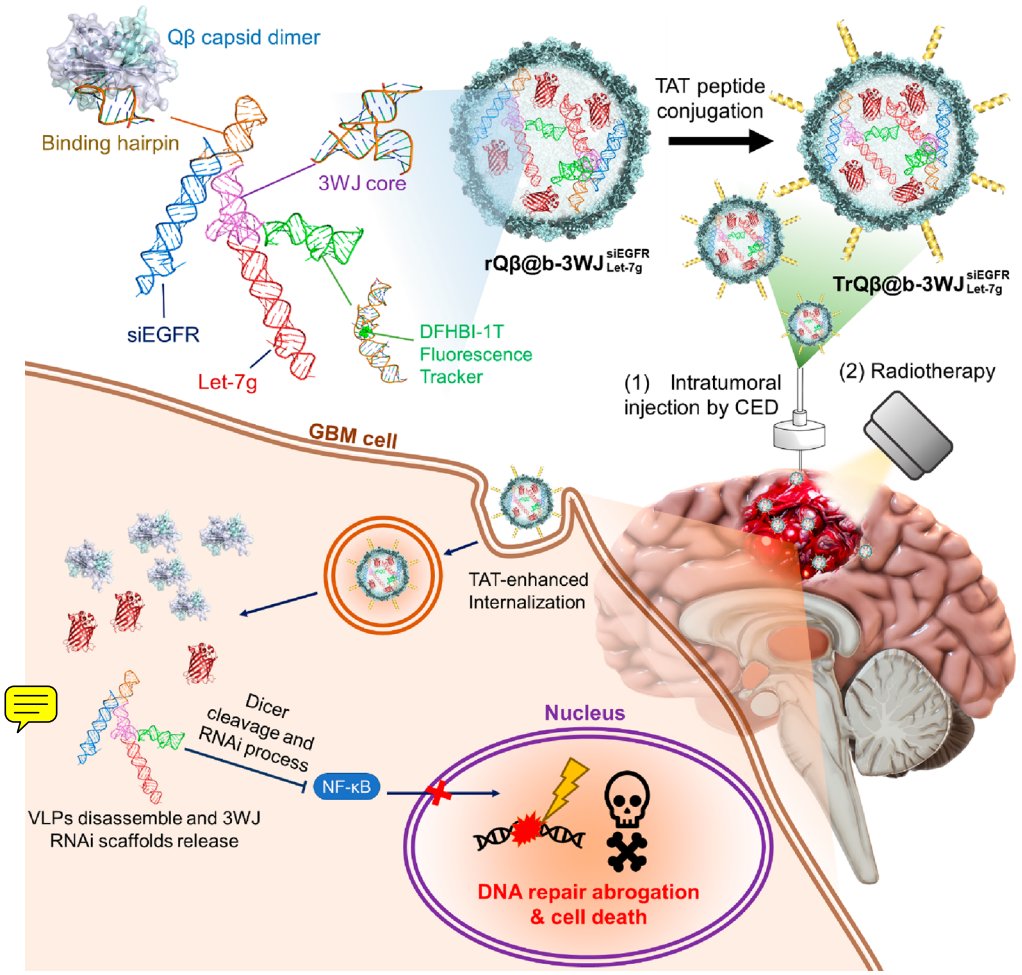

nanotechnology has been growing rapidly as a new generation platform for specific RNA target suppression.[10] As nanotechnology rapidly evolves, encapsulation of small interfering RNA (siRNA) in nanoparticles is a promising way to improve the effectiveness of siRNA for cancer treatment using lipid-,[11] polymer-,[12] metal-,[13] and virus-based[14] nanoparticles. However, the application of nanoparticle-encapsulated siRNA is confined by its low targeting efficiency, chemical and thermodynamic instability, and poor biocompatibility.[15] Currently, three-way junction (3WJ) RNA nanoparticles to deliver microRNA (miRNA)/silencing RNA (siRNA) have been reported to address thermodynamic instability issues.[16] The thermodynamically stable 3WJ motif derived from the bacteriophage phi29 DNA packaging motor (pRNA) core is composed of three oligos with a branched structure.[17] In particular, various sequences of siRNA can easily be incorporated into the branch of the pRNA-3WJ motifs via bottom-up self-assembly, which could be processed intracellularly by Dicer for multigene silencing. In addition, the RNA backbones with 2′-fluorine, 2′-*O*-methyl or 2′-amine modifications of U and C nucleotides render the RNAs resistant to RNase degradation or hydrolysis, enhancing their *in vivo* half-life while retaining authentic functions of the incorporated modules.[18,19] However, the chemical modification of RNAs will affect the folding properties and biological functions of RNA molecules[20] and will also cause higher production costs and lower production yields. Moreover, when the structure of the RNA becomes more complex to have more functions, the challenge above will be more critical.

Virus-like particles (VLPs) are constructed from viral structural proteins and capsomers and are free of any genetic material. They are genome-free versions of their viral nanoparticle (VNP) counterparts and are considered noninfectious, nontoxic, and nonimmunogenic.[21] Viruses are regarded as naturally occurring nucleic acid carriers, as they protect and carry their cargo.[22] Furthermore, drugs can also be infused, encapsulated, absorbed, or conjugated to the interior and exterior surfaces of coat protein interfaces through attachment to various functional groups offered by the protein structure.[23] This flexibility offers a variety of possibilities, including reversible binding of active molecules, protection within proteinaceous matrices, and specific targeting to the site of action. In addition, VLPs are devoid of their own genome; they can easily encapsulate nucleic acids and therefore have been broadly used for the delivery of genes as well as therapeutic nucleic acids. Tian et al. conjugated the transacting activation transduction (TAT) peptide onto the exterior surface of tobacco mosaic virus (TMV), which exhibited enhanced internalization for miRNA delivery.[24] Lam et al. also used cowpea chlorotic mottle virus (CCMV) VLPs carrying a cell penetrating peptide (M-lycotoxin peptide L17E) to enhance siRNA delivery into mammalian cells.[25] Our group

https://doi.org/10.1021/acsnano.3c01102
ACS Nano 2023, 17, 10407−10422

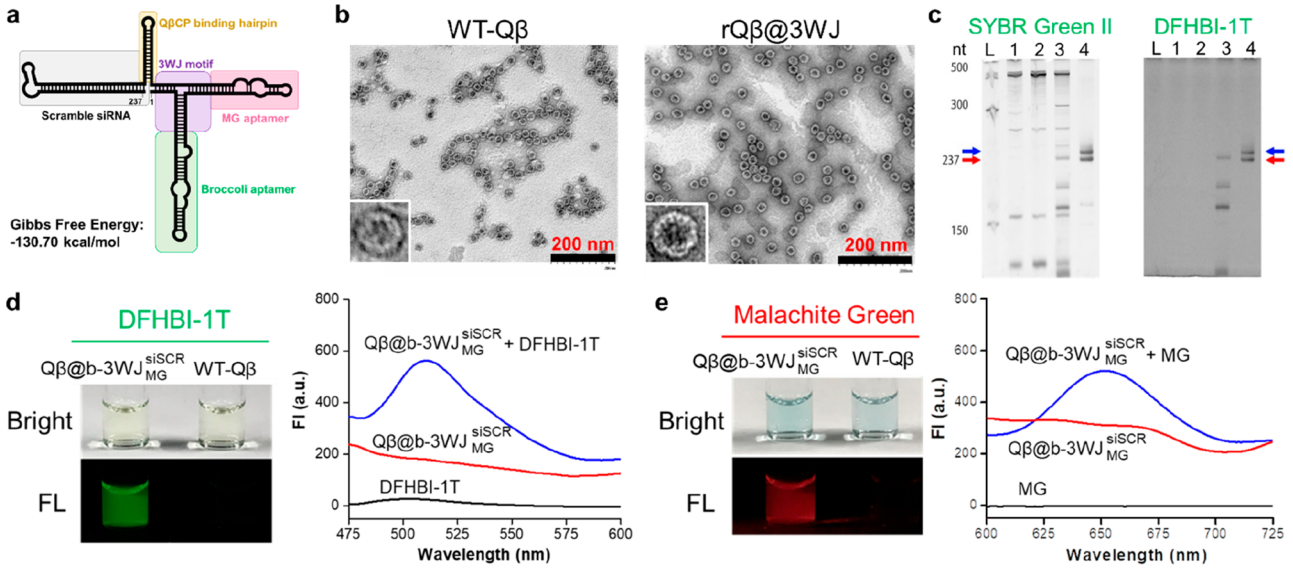

Figure 1. Design and characterization of the Qβ@b-3WJ$^{siSCR}_{MG}$. (a) The simulation of the secondary structure of the b-3WJ$^{siSCR}_{MG}$ scaffold. The simulated Gibbs free energy is −130.70 kcal/mol. (b) Transmission electron microscopy (TEM) image of WT-Qβ and rQβ@b-3WJ$^{siSCR}_{MG}$. Scale bar represents 200 nm. (c) Urea-PAGE electrophoresis analysis of the bioproduced b-3WJ$^{siSCR}_{MG}$ RNA scaffold. RNA extracted from *E. coli* was loaded in different lanes. The gel was stained with DFHBI-1T (right) for imaging the 3WJ RNA scaffold and SYBR green II (left) for imaging total RNA. L: ladder. Lane 1: control (*E. coli* without VLP production plasmid). Lane 2: *E. coli* without IPTG induction. Lane 3: *E. coli* with IPTG induction. Lane 4: *in vitro* transcription product. Red arrow: predicted RNA band (237 nt). Blue arrow: RNA polymerase read-through T7 terminator caused a larger fragment. (d) Bright view images, fluorescence images and fluorescence spectra for Qβ@b-3WJ$^{siSCR}_{MG}$ coincubated with DFHBI-1T. E_x = 418 nm (e) Bright view images, fluorescence images, and fluorescence spectra for Qβ@b-3WJ$^{siSCR}_{MG}$ coincubated with malachite green. E_x = 560 nm.

has constructed RNA-loaded Qβ VLPs with cell-penetrating peptides and apolipoprotein E (ApoE) modification to aid VLPs in crossing the blood-brain barrier and targeting malignant brain tumors.[26] However, the distribution of carried RNA in cells is difficult to monitor, and its processing by Dicer in cells cannot be monitored in real time by fluorescence microscopy thus far. At present, we can only use the Northern blotting method to analyze the status of RNA cleavage by Dicer enzyme, which is very complicated and time-consuming.

In this work, we proposed a broccoli light-up aptamer-included 3WJ RNA scaffold (b-3WJ) integrated with a nucleic acid bioproduction and self-packaging system to produce b-3WJ packaged red-fluorescent Qβ VLPs (rQβ@b-3WJ), followed by the conjugation of TAT peptide on the surface (TrQβ@b-3WJ) to enhance cellular internalization for highly efficient gene silencing. The benefits of this system are as follows: (1) biological production of all components and self-packaging, (2) multigene silencing, (3) real-time monitoring of intracellular RNA cleavage by Dicer enzyme using fluorescence microscopy, (4) RNA stability enhancement, and (5) great biosafety. Herein, we incorporated EGFR siRNA and miRNA Let-7g into the 3WJ RNA scaffold to produce rQβ@b-3WJ$^{siEGFR}_{Let\text{-}7g}$, which was delivered to tumor tissues through the convection-enhanced delivery (CED) method to overcome the blood-brain barrier (BBB) challenge and enhance radiotherapy in GBMs (Scheme 1 and Figure S1). Our study demonstrated that the designed TrQβ@b-3WJ$^{siEGFR}_{Let\text{-}7g}$ considerably enhanced antitumor efficacy via the synergistic effect of silencing the multigene related to DNA repair promotion, cell invasion ability, and radiotherapy, providing a promising approach for treating GBMs.

RESULTS

To impart better biosafety to the nucleic acid drug and considering that most manufacturing methods usually use liposomes to encapsulate naked RNA (i.e., siRNA, miRNA, mRNA), we designed a biological RNA production and self-packaging system, including bacterial Qβ phage capsid, b-3WJ RNA scaffold production, and then automatic packaging. The b-3WJ RNA scaffold consists of the following parts: (1) bacterial Qβ phage capsid binding hairpin, (2) three functional regions junction together with a three-way junction motif from bacteriophage Phi29 hexameric motor pRNA. Such structures help to assist RNA stabilization and facilitate cellular ingestion, resulting in therapeutic effects. To prove that the scaffold can be folded in the correct structure, we inserted scrambled siRNA (siSCR) at the left end, malachite green (MG) aptamer at the right end, and broccoli aptamer at the bottom of the scaffold, named b-3WJ$^{siSCR}_{MG}$ (Figure 1a). The b-3WJ$^{siSCR}_{MG}$ and Qβ capsid were coexpressed in a dual-plasmid *E. coli* expression system (Figure S2a). After induction using IPTG, the transcribed b-3WJ$^{siSCR}_{MG}$ with Qβ hairpin on the 5′ end and translated Qβ capsids self-assembled into Qβ VLPs with b-3WJ$^{siSCR}_{MG}$ self-packaged inside, named Qβ@b-3WJ$^{siSCR}_{MG}$. Packaging of the b-3WJ$^{siSCR}_{MG}$ in the capsid left the morphology of the Qβ@b-3WJ$^{siSCR}_{MG}$ unchanged and showed uniform size distribution when compared with the wild-type Qβ VLPs (WT-Qβ) using transmission electron microscopy (TEM) (Figure 1b); the diameter (Z-average) of Qβ@b-3WJ$^{siSCR}_{MG}$ was slightly increased to 30.6 ± 0.4 nm from 30.4 ± 0.2 nm (WT-Qβ) measured by dynamic light scattering (DLS), as shown in Figure S3.

The results demonstrated that b-3WJ$^{siSCR}_{MG}$ encapsulation did not affect the self-assembly of the Qβ capsid. To confirm that b-3WJ$^{siSCR}_{MG}$ was packaged inside Qβ VLPs, we extracted RNA

https://doi.org/10.1021/acsnano.3c01102
ACS Nano 2023, 17, 10407−10422

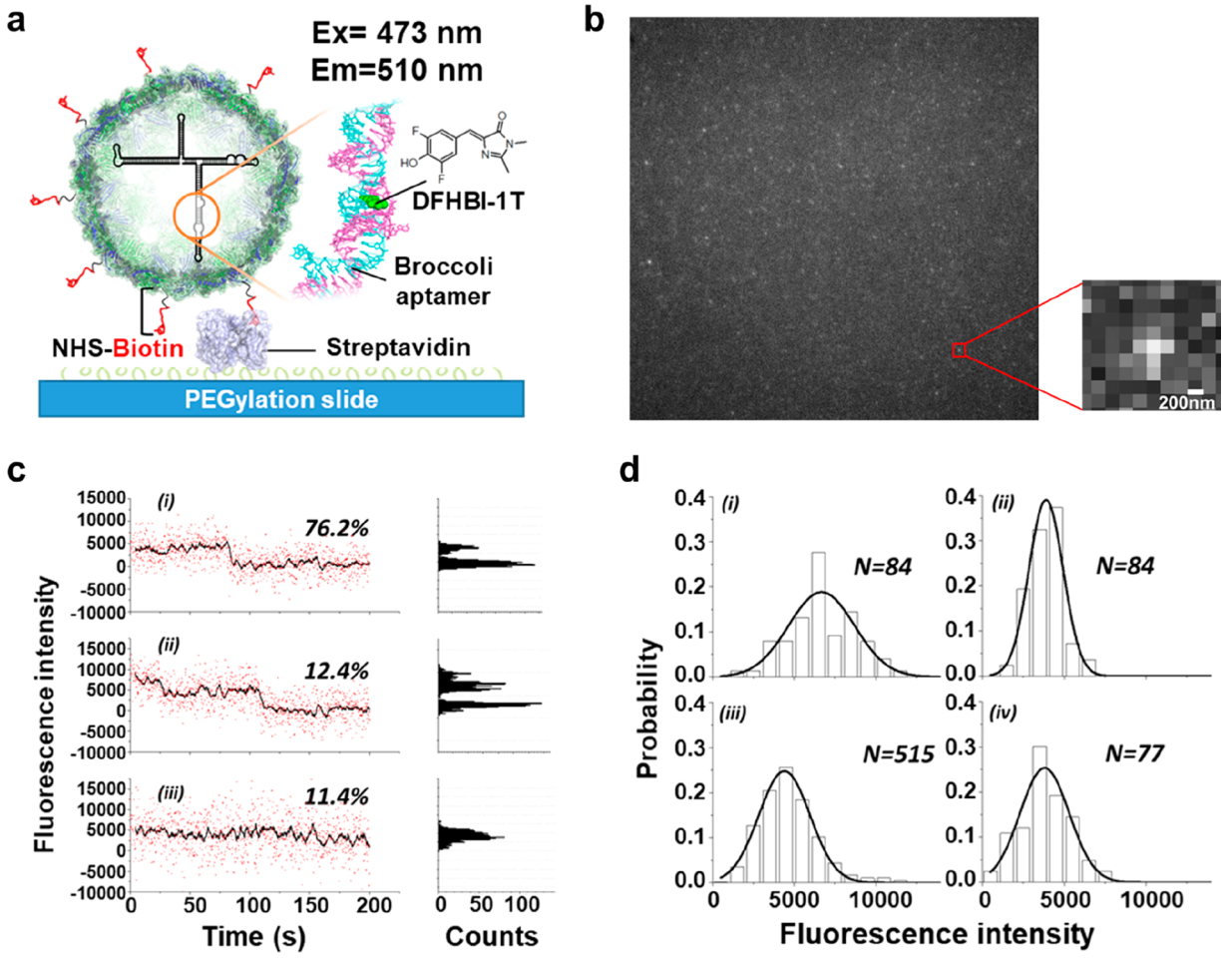

Figure 2. Quantification of RNA scaffolds in VLPs by single-molecule photobleaching imaging. (a) The experimental design to monitor the stepwise fluorescence photobleaching of individual Qβ@b-3WJ$_{MG}^{siSCR}$. (b) The fluorescence image of immobilized individual Qβ@b-3WJ$_{MG}^{siSCR}$ obtained under our system. The enlarged image indicates a single Qβ@b-3WJ$_{MG}^{siSCR}$ marked with a red square. (c) Representative fluorescence time trace of (*i*) one DFHBI-1T/RNA complex with one-step photobleaching (*P* = 76.2%), (*ii*) two DFHBI-1T/RNA complexes with two-step photobleaching (*P* = 12.4%), (*iii*) one DFHBI-1T/RNA complex without photobleaching within acquisition time window (*P* = 11.4%). (d) Fluorescence intensity histograms of (*i*) two DFHBI-1T/RNA complexes in one Qβ@b-3WJ$_{MG}^{siSCR}$ before the first-step photobleaching (6872 ± 1,892), (*ii*) two DFHBI-1T/RNA complexes in one Qβ@b-3WJ$_{MG}^{siSCR}$ before the second-step photobleaching (3889 ± 1,000), (*iii*) one DFHBI-1T/RNA complex in one Qβ@b-3WJ$_{MG}^{siSCR}$ before the first-step photobleaching (4360 ± 773), (*iv*) one DFHBI-1T/RNA complex in one Qβ@b-3WJ$_{MG}^{siSCR}$ without photobleaching within acquisition time window (3838 ± 1,400).

from Qβ@b-3WJ$_{MG}^{siSCR}$ and performed Urea-PAGE electrophoresis, followed by staining with SYBR green and DFHBI-1T. A band at 237 nt was significantly observed only in the groups of IPTG induction and *in vitro* transcription in both PAGEs stained with SYBR green (Figure 1c, left) and DFHBI-1T (Figure 1c, right). The results demonstrated that the b-3WJ$_{MG}^{siSCR}$ was successfully packaged inside, and the structure folded correctly because the broccoli aptamer in the scaffold reacted with DFHBI-1T to emit a green fluorescence band at 237 nt. Furthermore, the reactivity of Qβ@b-3WJ$_{MG}^{siSCR}$ with DFHBI-1T and MG was verified by incubating Qβ VLPs or Qβ@b-3WJ$_{MG}^{siSCR}$ with DFHBI-1T and MG solution. As shown in Figure 1d and 1e, only Qβ@b-3WJ$_{MG}^{siSCR}$ can react with DFHBI-1T and MG to exhibit green fluorescence (E_m: 510 nm) and red fluorescence (E_m: 652 nm), indicating that the packaged b-3WJ$_{MG}^{siSCR}$ can still react with the substrate to emit fluorescence for real-time cellular RNA process status monitoring. Thus, we can react the *in vitro* transcribed b-3WJ RNAs with DFHBI-1T to quantify the amount of b-3WJ RNAs packaged in Qβ VLPs by measuring the fluorescence intensity (FI) at 510 nm (Figure S4). The results showed that the FI increased in proportion to the amount of b-3WJ RNAs.

Several approaches have been developed to quantify a number of fluorophores, such as fluorescence fluctuation spectroscopy for moving complexes[27] or localization fluorescence imaging systems, including photoactivated localization microscopy/stochastic optical reconstruction microscopy[28] and single-molecule photobleaching (SMPB) imaging.[29] To quantify the b-3WJ RNA molecules within individual Qβ VLPs, the SMPB system was adapted here. Individual b-3WJ$_{MG}^{siSCR}$ were immobilized on polyethylene glycol (PEG) ylated glass through a specific biotin−streptavidin interaction, and the fluorescence signals from DFHBI-1T/b-3WJ RNA complexes were acquired using a home-built TIRFM imaging system (Figure 2a). Upon 473 nm excitation, fluorescence signals from individual Qβ@b-3WJ$_{MG}^{siSCR}$ were obtained. The fluorescence spot acquired and analyzed in our system exhibited a diffraction limit (Figure 2b), representing the signal from individual Qβ@b-3WJ$_{MG}^{siSCR}$. All acquired fluorescence intensity time traces can be classified into three different

https://doi.org/10.1021/acsnano.3c01102
ACS Nano 2023, 17, 10407−10422

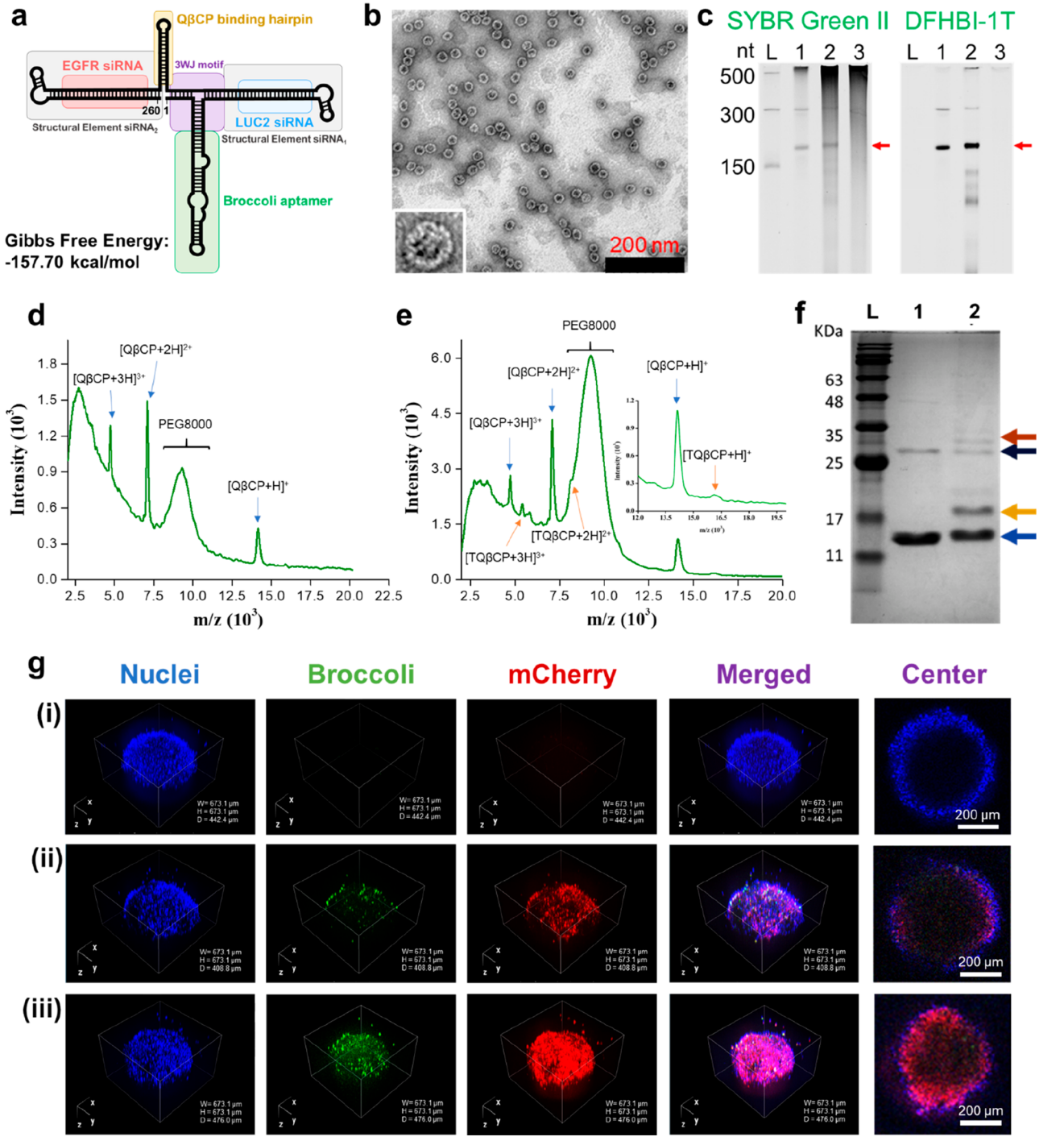

Figure 3. Design and characterization of rQβ@b-3WJ$^{siEGFR}_{siLUC}$. (a) The simulation of the secondary structure of the b-3WJ$^{siEGFR}_{siLUC}$ scaffold. The simulated Gibbs free energy is −157.70 kcal/mol. (b) TEM image of rQβ@b-3WJ$^{siEGFR}_{siLUC}$. Scale bar represents 200 nm. (c) Urea-PAGE electrophoresis analysis of bioproduced b-3WJ$^{siEGFR}_{siLUC}$RNA scaffold. RNAs extracted from Qβ VLPs was loaded in different lanes. The gel was stained with DFHBI-1T (right) for imaging the 3WJ RNA scaffold and SYBR green II (left) for imaging total RNA. L: ladder. Lane 1: *in vitro* transcription product. Lane 2: rQβ@b-3WJ$^{siEGFR}_{siLUC}$. Lane 3: Qβ VLPs. Red arrow: predicted RNA band (260 nt). The band vaguely visible at approximately 300 nt indicates that the T7 terminator caused a larger fragment. (d) MALDI-TOF Ms spectrum of Qβ@b-3WJ$^{siEGFR}_{siLUC}$. (e) MALDI-TOF Ms spectrum of TQβ@b-3WJ$^{siEGFR}_{siLUC}$. (f) Characterization of prepared Qβ@b-3WJ$^{siEGFR}_{siLUC}$ (Lane 1) and TQβ@b-3WJ$^{siEGFR}_{siLUC}$ (Lane 2) by 15% SDS-PAGE. The molecular weight of the QβCP monomer is 14.4 kDa. Blue arrow: QβCP monomer; dark blue arrow: QβCP dimer; yellow arrow: QβCP monomer conjugated with TAT peptide; brown arrow: QβCP dimer conjugated with TAT peptide. (g) Three-dimensional U87MG cell spheroid uptake of (i) PBS (control), (ii) rQβ@b-3WJ$^{siEGFR}_{siLUC}$, and (iii) TrQβ@b-3WJ$^{siEGFR}_{siLUC}$. Blue channel: Hoechst 33342-stained cell nucleus; green channel: DFHBI-1T incubated 3WJ RNAs containing broccoli aptamer; red channel: mCherry protein (rQβ VLPs), merge: the merged image of the three channels above. Scale bar: 200 μm.

patterns: one-step photobleaching with a probability of 76.2%, two-step photobleaching with a probability of 12.4%, and no significant photobleaching during the acquisition time window with a probability of 11.4% (Figure 2c). Averaged intensity

https://doi.org/10.1021/acsnano.3c01102
ACS Nano 2023, 17, 10407−10422

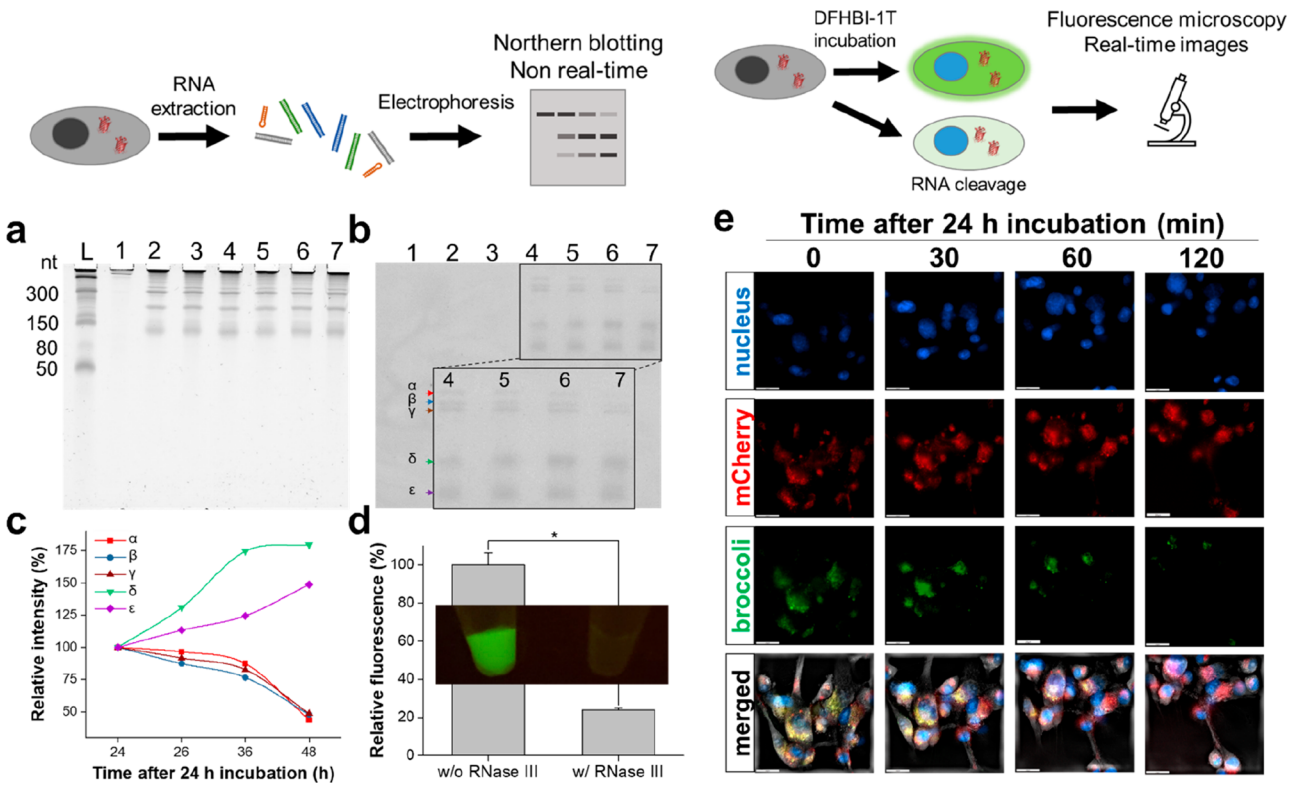

Figure 4. RNA scaffold degradation *in vitro*. (a–c) Northern blotting for total RNA extracted from treated cells. (a) SYBR green II-stained 10% Urea-PAGE. Lane L: low range ssRNA ladder, Lane 1: RNA extracted from WT-Qβ (negative control), Lane 2: blank (untreated cells), 3: TrQβ VLPs, 4: TrQβ@b-3WJ$^{siEGFR}_{siLUC}$ (24 h), Lane 5: TrQβ@ b-3WJ$^{siEGFR}_{siLUC}$ (26 h), Lane 6: TrQβ@b-3WJ$^{siEGFR}_{siLUC}$ (36 h), Lane 7: TrQβ@b-3WJ$^{siEGFR}_{siLUC}$ (48 h). (b) Northern blotting for (a) Urea-PAGE by biotin-conjugated siEGFR complementary DNA probe. b-inner box is the detailed image of the black box in (b); α to ε indicate different sizes of RNA segments. (c) Quantitation of different lanes in (b) using ImageJ. (d) RNase III process assay of relative fluorescence intensity and image comparison of naked 3WJ RNAs before and after the RNase III process. Values are expressed as the means ± standard deviations (SDs) (n = 3). *Indicates a significant difference (Student's t-test, *p < 0.05). (e) Real-time image of TrQβ@b-3WJ$^{siEGFR}_{siLUC}$-treated cells after DFHBI-1T incubation. Scale bar represents 20 μm. Blue: Hoechst 33342-stained nucleus, red: mCherry protein in TrQβ@b-3WJ$^{siEGFR}_{siLUC}$, green: broccoli aptamer after incubation with DFHBI-1T and merged is the merge of all channels with bright view.

values of 6872 ± 1892 and 3889 ± 1000 were obtained for the first-step and second-step photobleaching of individual Qβ@b-3WJ$^{siSCR}_{MG}$ containing two DFHBI-1T/b-3WJ RNA complexes, respectively (Figure 2d (i)-(ii)). For individual Qβ@b-3WJ$^{siSCR}_{MG}$ containing a single DFHBI-1T/b-3WJ RNA complex, an averaged intensity value of 4360 ± 773, similar to the value obtained in the second-step photobleaching of Qβ@b-3WJ$^{siSCR}_{MG}$ containing two DFHBI-1T/b-3WJ RNA complexes, was obtained (Figure 2d (iii)). For molecules exhibiting no significant photobleaching, an averaged intensity value of 3838 ± 1400 was obtained, indicating the signal coming from a single DFHBI-1T/b-3WJ RNA complex in individual Qβ@b-3WJ$^{siSCR}_{MG}$ (Figure 2d (iv)). Based on SMPB analysis, 87.6% of Qβ@b-3WJ$^{siSCR}_{MG}$ contains one DFHBI-1T/b-3WJ RNA complex in one Qβ VLP, while 12.4% of Qβ@b-3WJ$^{siSCR}_{MG}$ contains two DFHBI-1T/b-3WJ RNA complexes in one Qβ VLP.

Next, we verified the effectiveness of Qβ@b-3WJ in gene silencing by replacing siSCR with EGFR siRNA (siEGFR) and MG aptamer with luciferase siRNA (siLUC) in the 3WJ RNA scaffold, named rQβ@b-3WJ$^{siEGFR}_{siLUC}$ (Figure 3a and Figure S2b). After IPTG induction and purification, the extracted rQβ@b-3WJ$^{siEGFR}_{siLUC}$ showed a uniform spherical shape with a diameter of approximately 31.4 ± 0.5 nm, proving again that mCherry protein and b-3WJ$^{siEGFR}_{siLUC}$ packaging do not affect the self-assembly of Qβ phage capsids (Figure 3b). SYBR green II- and DFHBI-1T-stained urea-polyacrylamide gel electrophoresis (PAGE) also confirmed that b-3WJ$^{siEGFR}_{siLUC}$ was indeed packaged inside Qβ VLPs by observing the band at 260 nt only in the *in vitro* transcription and Qβ@b-3WJ$^{siEGFR}_{siLUC}$ groups (Figure 3c). Furthermore, Qβ@b-3WJ$^{siEGFR}_{siLUC}$ was suspended in DFHBI-1T solution, and a significant fluorescence peak at 611 nm was obtained upon 473 nm excitation (Figure S5), indicating that the copackaged mCherry protein would not interfere with the reactivity of broccoli aptamer with DFHBI-1T. However, the emission of DFHBI-1T shifted to 575 nm from 510 nm, most likely because the DFHBI-1T (donor) emission spectrum overlaps with the mCherry (acceptor) excitation spectrum to excite the packaged mCherry. The results indicated that the mCherry protein and b-3WJ$^{siEGFR}_{siLUC}$ were successfully produced by *E. coli* and copackaged in Qβ VLPs.

Furthermore, the TAT peptide was modified on the surface of rQβ@b-3WJ$^{siEGFR}_{siLUC}$ to enhance cellular internalization, most likely because the TAT peptide originates from the HIV transactivator of transcription protein, which has demonstrated excellent potential in translocating across the plasma membrane of various cell types. Successful TAT peptide conjugation was confirmed by Matrix-assisted laser desorption ionization–time-of-flight mass spectrometry (MALDI-TOF MS) and sodium dodecyl sulfate (SDS)-PAGE. The representative MALDI-TOF MS spectra of Qβ@b-3WJ$^{siEGFR}_{siLUC}$

https://doi.org/10.1021/acsnano.3c01102
ACS Nano 2023, 17, 10407–10422

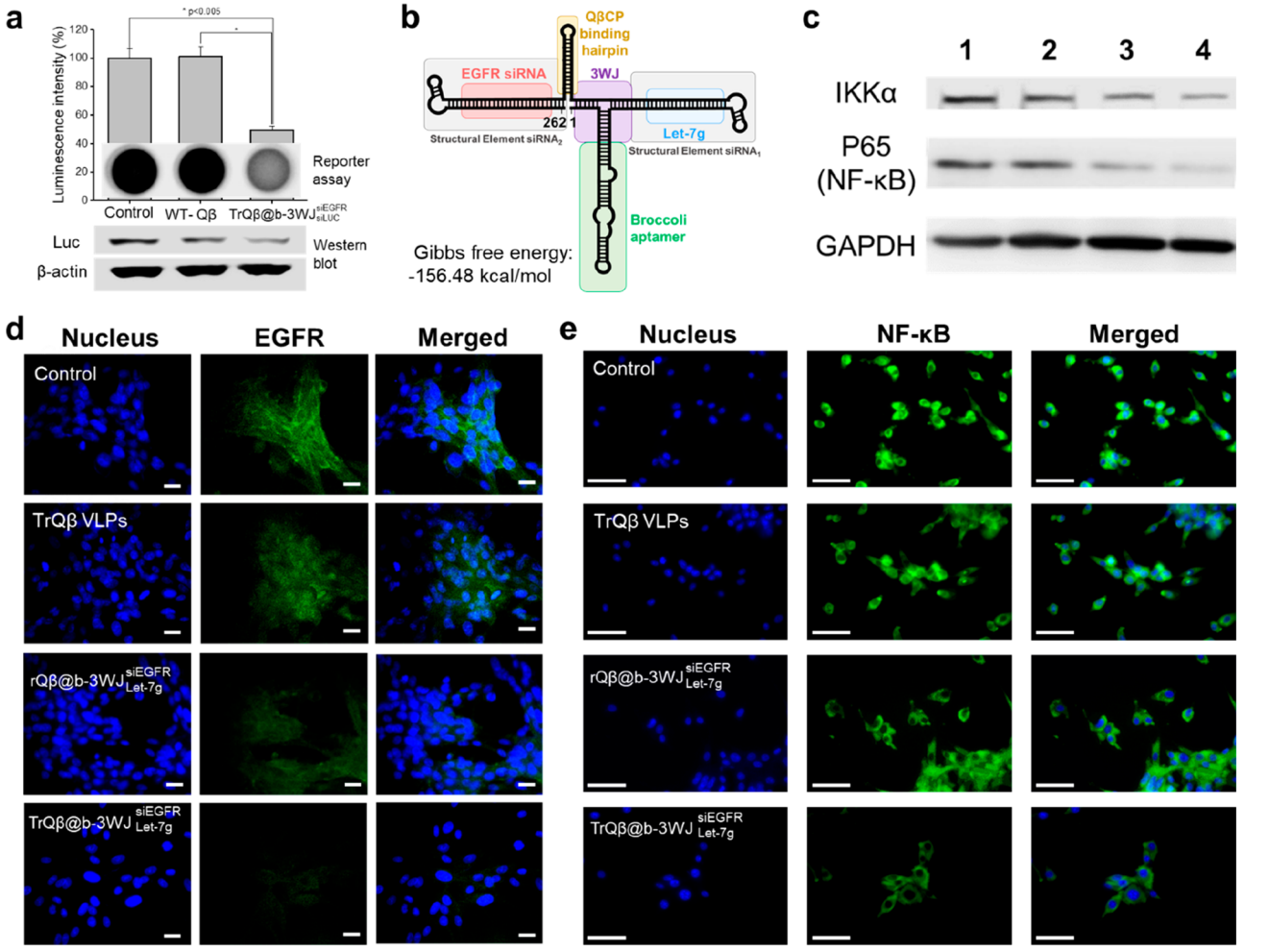

Figure 5. ***In vitro*** **functional analysis of b-3WJ RNA scaffolds. (a) Luciferase reporter assay and luciferase Western blot analysis of U87MG cells after treatment with WT-Q*β*** **or TrQ*β*@b-3WJ$^{siEGFR}_{siLUC}$. Values are expressed as the means ± SDs (*n* = 3). *Indicates a significant difference (Student's *t*-test, **p* < 0.05). (b) The simulation of the secondary structure of b-3WJ$^{siEGFR}_{Let\text{-}7g}$ scaffold. The simulated Gibbs free energy is −156.48 kcal/mol. (c) IKK*α* and NF-*κ*B (p65) protein Western blot analysis of U87MG cells after treatment with PBS (Lane 1), 1 *μ*M of TrQ*β* VLPs (Lane 2) or rQ*β*@b-3WJ$^{siEGFR}_{Let\text{-}7g}$ (Lane 3) or TrQ*β*@b-3WJ$^{siEGFR}_{Let\text{-}7g}$ (Lane 4). (d) Immunofluorescence staining images of EGFR expression in U87MG cells treated with TrQ*β* VLPs, rQ*β*@b-3WJ$^{siEGFR}_{siLUC}$ or TrQ*β*@b-3WJ$^{siEGFR}_{siLUC}$ for 72 h. Scale bar represents 20 *μ*m. (e) Immunofluorescence staining images of NF-*κ*B expression in U87MG cells treated with TrQ*β* VLPs, rQ*β*@b-3WJ$^{siEGFR}_{siLUC}$ or TrQ*β*@b-3WJ$^{siEGFR}_{siLUC}$ for 72 h. Scale bar represents 60 *μ*m.**

and TQ*β*@b-3WJ$^{siEGFR}_{siLUC}$ are shown in Figure 3d and 3e. For TQ*β*@b-3WJ$^{siEGFR}_{siLUC}$, new peaks appeared at *m*/*z* 5390, *m*/*z* 8095, and *m*/*z* 16505 VLPs belong to one $3H^+$ ionized TAT-conjugated Q*β* capsid protein (TQ*β*CP), $2H^+$ ionized TQ*β*CP, and H^+ ionized TQ*β*CP compared with Q*β*@b-3WJ$^{siEGFR}_{siLUC}$, indicating that TAT peptides were indeed conjugated on the surface of Q*β*@b-3WJ$^{siEGFR}_{siLUC}$. The results were also confirmed by SDS-PAGE, and new bands appeared at 17.1 kDa (single TAT peptide conjugation on one Q*β* capsid protein monomer) and 19.8 kDa (two TAT peptides conjugated on one Q*β* capsid protein monomer) after TAT peptide conjugation (Figure 3f, Lane 2) compared with nonmodified Q*β*@b-3WJ$^{siEGFR}_{siLUC}$ (Figure 3f, Lane 1), thereby proving the successful conjugation of TAT peptides on Q*β*@b-3WJ$^{siEGFR}_{siLUC}$ to form TQ*β*@b-3WJ$^{siEGFR}_{siLUC}$. Subsequently, we incubated the U87MG cells with rQ*β*@b-3WJ$^{siEGFR}_{siLUC}$ and TrQ*β*@b-3WJ$^{siEGFR}_{siLUC}$ to compare their ability of getting into the cells. The distributions of TrQ*β* VLPs (red fluorescence) and b-3WJ$^{siEGFR}_{siLUC}$ (green fluorescence) were both markedly higher in the whole tumor spheroid and can penetrate deeper into the tumor spheroid than in the absence of TAT peptide-modified rQ*β*@b-3WJ$^{siEGFR}_{siLUC}$ (Figure 3g), indicating that TAT peptides can indeed effectively increase tumor cell uptake and penetration. This enhanced adsorption and transportation was essential for inhibiting tumor growth.

When the RNA duplex is delivered into the cells, the ribonuclease (RNase) III enzyme Dicer processes double-stranded RNAs (dsRNAs) into 21−22-nt-long duplexes with 2-nt 3′overhangs, guiding sequence-specific degradation of complementary mRNAs (mRNAs) once incorporated into the RNA-induced silencing complex (RISC).[30] Dicer-2 (Dcr-2) processes long double-stranded precursors and generates siRNAs, while Dicer-1 (Dcr-1) processes pre-miRNAs into mature miRNAs.[31] To date, Northern blotting is a promising tool to observe the intracellular cleavage status of RNA with Dicer enzyme. In this study, to determine when the delivered b-3WJ$^{siEGFR}_{siLUC}$ is cleaved in cells by Dicer enzyme, the extracted RNAs from cells with different treatments were analyzed by Northern blotting. From 10% Urea-PAGE stained with SYBR green II, the RNA signal was detected in all cell samples with

https://doi.org/10.1021/acsnano.3c01102
ACS Nano 2023, 17, 10407−10422

different treatments (Figure 4a, Lanes 2−7). Using a biotin-conjugated DNA probe complementary to the siEGFR strand of b-3WJ$^{siEGFR}_{siLUC}$, only the samples from the cells treated with TrQβ@b-3WJ$^{siEGFR}_{siLUC}$ still exhibited an obvious RNA signal (Figure 4b, Lanes 4−7), indicating that TrQβ@b-3WJ$^{siEGFR}_{siLUC}$ can be internalized into cells and release b-3WJ$^{siEGFR}_{siLUC}$. Furthermore, the delivered b-3WJ$^{siEGFR}_{siLUC}$ began to be cleaved into small fragments as the incubation time increased. By comparison to the sample from the cells incubated with TrQβ@b-3WJ$^{siEGFR}_{siLUC}$ for 24 h (Figure 4b, Lane 4), the large fragments of b-3WJ$^{siEGFR}_{siLUC}$ significantly decreased, while the small fragments significantly increased after an additional 48 h of incubation (Figure 4b, Lane 7 and Figure 4c), indicating that the delivered b-3WJ$^{siEGFR}_{siLUC}$ could be released from TrQβ@b-3WJ$^{siEGFR}_{siLUC}$ and then cleaved by the Dicer enzyme to specifically degrade the complementary mRNAs. However, Northern blotting is not only complicated and time-consuming but also cannot monitor the RNA cleavage status in real time. Otherwise, our designed b-3WJ$^{siEGFR}_{siLUC}$ can react with DFHBI-1T to emit green fluorescence when its structure is intact, but the broccoli aptamer loses its reactivity with DFHBI-1T when the b-3WJ$^{siEGFR}_{siLUC}$ is cleaved by Dicer enzyme, resulting in a decrease in green fluorescence. As proof, we treated the *in vitro* transcribed b-3WJ$^{siEGFR}_{siLUC}$ with a ShortCut RNase III kit at 37 °C for 20 min, and the green fluorescence was significantly weakened compared to the green fluorescence of the nontreated b-3WJ$^{siEGFR}_{siLUC}$ (Figure 4d), indicating that b-3WJ$^{siEGFR}_{siLUC}$ can be cleaved into small fragments by the Dicer enzyme and lose its reactivity with DFHBI-1T. Subsequent incubation of TrQβ@b-3WJ$^{siEGFR}_{siLUC}$ with U87MG cells in the presence of DFHBI-1T allowed us to monitor the distribution of TrQβ@b-3WJ$^{siEGFR}_{siLUC}$ and the cleavage status of b-3WJ$^{siEGFR}_{siLUC}$ simultaneously in cells using a fluorescence microscope. As shown in Figure 4e, a large amount of TrQβ@b-3WJ$^{siEGFR}_{siLUC}$ was endocytosed into U87MG cells to exhibit strong red fluorescence (TrQβ VLPs) and green fluorescence (b-3WJ$^{siEGFR}_{siLUC}$) after 24 h of incubation, indicating the b-3WJ$^{siEGFR}_{siLUC}$ can be indeed delivered into tumor cells. The green fluorescence in cells gradually disappeared with increasing incubation time, while the intracellular red fluorescence did not decrease at all. The results indicated that b-3WJ$^{siEGFR}_{siLUC}$ can be successfully delivered into cells by TrQβ VLPs and that its cleavage status with the Dicer enzyme can easily be monitored by fluorescence microscopy in real time.

RNA stability is one of the important factors affecting the success or failure of RNA interference (RNAi) therapy. However, packaging in rQβ VLPs protects b-3WJ$^{siEGFR}_{siLUC}$ against urea-mediated denaturation and RNase A-mediated cleavage. We incubated rQβ@b-3WJ$^{siEGFR}_{siLUC}$ with urea and RNase A and then mixed it with DFHBI-1T to assess the integrity of the b-3WJ$^{siEGFR}_{siLUC}$ structure. After 144 h of incubation in the biological urea concentration (10 mM) urea at 37 °C, the b-3WJ$^{siEGFR}_{siLUC}$ within rQβ VLPs was approximately 80% intact. In contrast, less than 10% of naked b-3WJ$^{siEGFR}_{siLUC}$ was intact under the same conditions (Figure S6a). Similarly, nearly 100% of rQβ VLPs packaged with b-3WJ$^{siEGFR}_{siLUC}$ remained intact after 400 s at an RNase A concentration of 0.1 mg/mL, most likely because rQβ VLPs protect packaged b-3WJ$^{siEGFR}_{siLUC}$ from degradation by nucleases, which are larger than the pore size of the rQβ VLPs.[32] There was no detectable intact b-3WJ$^{siEGFR}_{siLUC}$ remaining after the same incubation time for naked b-3WJ$^{siEGFR}_{siLUC}$ under the same conditions (Figure S6b). Taken together, the results show that packaged RNA in rQβ VLPs degrades slowly at 37 °C in the presence of urea and RNase A without complex structural modifications that has considerable potential for the development of nucleic acid drugs.

Next, we assessed the gene silencing ability of TrQβ@b-3WJ$^{siEGFR}_{siLUC}$ to EGFR and luciferase in luciferase-expressing U87MG cells. Incubation of luciferase-expressing U87MG cells with TrQβ@b-3WJ$^{siEGFR}_{siLUC}$ decreased the expression of luciferase, as shown by bioluminescence imaging and Western blot analysis. The results show that incubation in 1 μM TrQβ@b-3WJ$^{siEGFR}_{siLUC}$ for 72 h efficiently knocked down approximately 55% of luciferase expression compared with the control and WT-Qβ-treated groups (Figure 5a). Moreover, TrQβ@b-3WJ$^{siEGFR}_{siLUC}$ also showed excellent inhibition of EGFR expression, and approximately 91% expression of EGFR was suppressed in U87MG cells compared with the control group (Figure S7). The overall results indicate that inhibition is caused by delivered b-3WJ$^{siEGFR}_{siLUC}$, but not by TrQβ VLPs, and the TrQβ@b-3WJ$^{siEGFR}_{siLUC}$ can simultaneously downregulate two target genes.

Nuclear factor kappa B (NF-κB) is well established to be activated in response to a variety of DNA lesions, such as TMZ-induced S_N1 methylation, cisplatin-induced DNA cross-linking, and IR-induced double-strand breaks (DSBs).[33,34] Inhibition of NF-κB increases the sensitivity of cancer cells to the apoptotic action of chemotherapeutic agents and radiation exposure.[35] In humans, the IκB kinase (IKK) complex serves as the master regulator for the activation of NF-κB by various stimuli. The IKK complex consists of IKKα and IKKβ, which form the catalytic subunit, and the regulatory subunit IKKγ.[36,37] Previous reports pointed out that the down-regulation of EGFR expression would affect RIPK1/TAK-1/TRAF2 message transmission and thus inhibit the expression of the IKK complex.[38] Let-7g cleaves IKKα mRNA and may play an important role in the response to IR through the inhibition of NF-κB.[39] Therefore, we replaced siLUC with Let-7 g miRNA in the 3WJ RNA scaffold and performed the production, named rQβ@b-3WJ$^{siEGFR}_{Let\text{-}7g}$ (Figure 5b). The obtained rQβ@b-3WJ$^{siEGFR}_{Let\text{-}7g}$ modified with TAT peptides on the surface (TrQβ@b-3WJ$^{siEGFR}_{Let\text{-}7g}$) can still emit green fluorescence in the presence of DFHBI-1T, indicating that the structure of b-3WJ$^{siEGFR}_{Let\text{-}7g}$ still folded correctly after sequence exchange (Figure S8) and could be protected from RNase A degradation for more than 1 h (Figure S9). To verify the effectiveness of TrQβ@b-3WJ$^{siEGFR}_{Let\text{-}7g}$ in the downregulation of NF-κB for enhanced radiotherapy, the expression of EGFR and NF-κB and the translocation of NF-κB to the nucleus were confirmed by Western blotting and immunofluorescence staining. The results show that both rQβ@b-3WJ$^{siEGFR}_{Let\text{-}7g}$ and TrQβ@b-3WJ$^{siEGFR}_{Let\text{-}7g}$ can downregulate the expression of IKKα and NF-κB (p65) compared with control and TrQβ VLPs groups. However, the TrQβ@b-3WJ$^{siEGFR}_{Let\text{-}7g}$ showed higher gene silencing efficiency for IKKα and NF-κB (P65) than rQβ@b-3WJ$^{siEGFR}_{Let\text{-}7g}$ because the TAT peptides on TrQβ@b-3WJ$^{siEGFR}_{Let\text{-}7g}$ effectively increase tumor cell uptake and penetration (Figure 5c). Subsequently, the gene silencing efficiency of TrQβ@b-3WJ$^{siEGFR}_{Let\text{-}7g}$ for EGFR and NF-κB in U87MG cells was also confirmed by immunofluorescence staining. The EGFR expression (green fluorescence) on cell membrane was significantly downregulated by TrQβ@b-3WJ$^{siEGFR}_{Let\text{-}7g}$ and much lower than that by rQβ@b-3WJ$^{siEGFR}_{Let\text{-}7g}$ (Figure 5d). Not only that, the translocation of NF-κB to the nucleus of U87MG cells was also significantly inhibited (no green fluorescence exhibited in nucleus) after treatment with TrQβ@b-3WJ$^{siEGFR}_{Let\text{-}7g}$

https://doi.org/10.1021/acsnano.3c01102
ACS Nano 2023, 17, 10407−10422

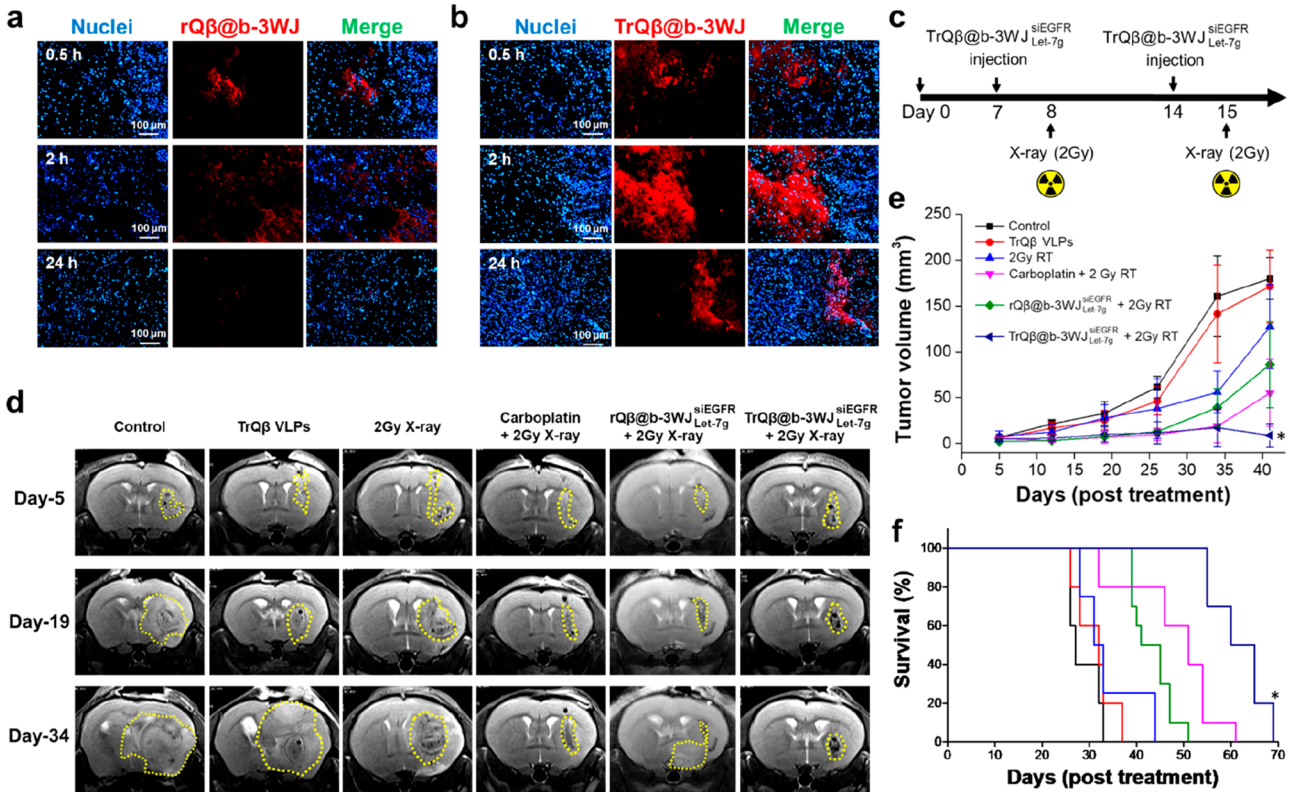

Figure 6. ***In vivo*** **tumor inhibition and survival studies. (a) Distribution of delivered rQ*β*@b-3WJ$^{siEGFR}_{Let\text{-}7g}$ in brain tumor tissue after 0.5, 2, and 24 h via CED infusion. (b) Distribution of delivered TrQ*β*@b-3WJ$^{siEGFR}_{Let\text{-}7g}$ in brain tumor tissue after 0.5, 2, and 24 h via CED infusion. (c) Treatment protocols assessing multigene silencing-enhanced radiotherapy. (d) Brain magnetic resonance imaging (MRI) images of NU mice after treatments. Control: PBS injection only. TrQ*β* VLPs: Q*β* VLP (5 *μ*M) injection only. Radiotherapy: 2Gy X-ray irradiation only. Carboplatin + 2Gy X-ray irradiation: carboplatin (10 mg/mL) injection followed by 2Gy X-ray irradiation. rQ*β*@b-3WJ$^{siEGFR}_{Let\text{-}7g}$ (5 *μ*M) + 2Gy X-ray irradiation: rQ*β*@b-3WJ$^{siEGFR}_{Let\text{-}7g}$ (5 *μ*M) injection followed by 2Gy X-ray irradiation. TrQ*β*@b-3WJ$^{siEGFR}_{Let\text{-}7g}$ (5 *μ*M) + 2Gy X-ray irradiation: TrQ*β*@b-3WJ$^{siEGFR}_{Let\text{-}7g}$ (5 *μ*M) injection followed by 2Gy X-ray irradiation. (e) Tumor volume measurement by MRI for mice after different treatments. *Indicates a significant difference (Student's *t*-test, *$p < 0.05$) of TrQ*β*@b-3WJ$^{siEGFR}_{Let\text{-}7g}$ (5 *μ*M) + 2Gy X-ray irradiation to all other treatment groups on Day 41. There is no significant tumor volume difference between all groups on Day 5. (f) Kaplan−Meier survival curves for mice that received different treatments. Values are expressed as the means ± SDs ($n = 10$). *Indicates a significant difference (log-rank test, *$p < 0.05$) of TrQ*β*@b-3WJ$^{siEGFR}_{Let\text{-}7g}$ (5 *μ*M) + 2Gy X-ray irradiation to all other treatment groups.**

compared with control (PBS), TrQ*β* VLPs, and rQ*β*@b-3WJ$^{siEGFR}_{Let\text{-}7g}$ treated groups (Figure 5e). We then quantified the gene silencing efficiency of rQ*β*@b-3WJ$^{siEGFR}_{Let\text{-}7g}$ and TrQ*β*@b-3WJ$^{siEGFR}_{Let\text{-}7g}$ for EGFR, IKK*α*, and NF-*κ*B in U87MG cells using flow cytometry (Figure S10). The results showed that the TrQ*β*@b-3WJ$^{siEGFR}_{Let\text{-}7g}$ could inhibit approximately 52.05% of EGFR protein expression (28.18% for rQ*β*@b-3WJ$^{siEGFR}_{Let\text{-}7g}$), 36.87% of IKK*α* protein expression (25.60% for rQ*β*@b-3WJ$^{siEGFR}_{Let\text{-}7g}$), and 36.37% of NF-*κ*B protein expression (13.31% for rQ*β*@b-3WJ$^{siEGFR}_{Let\text{-}7g}$) compared with the control group. These results indicating that TrQ*β*@b-3WJ$^{siEGFR}_{Let\text{-}7g}$ can deliver more b-3WJ$^{siEGFR}_{Let\text{-}7g}$ than rQ*β*@b-3WJ$^{siEGFR}_{Let\text{-}7g}$ into U87MG cells to significantly enhance the efficiency of radiotherapy by effectively downregulating the expression of NF-*κ*B because the overexpression of NF-*κ*B promotes DNA repair.[40] In addition, inhibition of EGFR and IKK complex expression by TrQ*β*@b-3WJ$^{siEGFR}_{Let\text{-}7g}$ not only inhibited DNA repair but also effectively suppressed cell migration by 40−50% in a wound-healing assay (Figure S11) and inhibited the invasion rate by approximately 60% in a trans-well assay (Figure S12). The results were also confirmed by observing cell progression after pretreatment with TrQ*β*@b-3WJ$^{siEGFR}_{Let\text{-}7g}$, showing that the cell progression rate of pretreated U87MG cells was significantly slower than the cell projection rate of the control group (without any treatment), WT-Q*β*, and rQ*β*@b-3WJ$^{siEGFR}_{Let\text{-}7g}$ treatment groups (Figure S13). According to the above results, TrQ*β*@b-3WJ$^{siEGFR}_{Let\text{-}7g}$ (with TAT peptide conjugation) have been proven to have superior cell penetration efficiency than rQ*β*@b-3WJ$^{siEGFR}_{Let\text{-}7g}$ (without TAT peptide conjugation). Therefore, we then investigated the *in vitro* synergistic effect of EGFR/IKK*α* gene silencing and X-ray irradiation (Figure S14). The cell viability of U87MG cells through the pretreatment with TrQ*β*@b-3WJ$^{siEGFR}_{Let\text{-}7g}$ for 72 h followed by 2Gy X-ray irradiation was decreased to 8.7 ± 3.4% compared with the 2Gy X-ray irradiated group (cell viability: 41.6 ± 4.9%) and rQ*β*@b-3WJ$^{siEGFR}_{Let\text{-}7g}$ + 2Gy X-ray irradiated group (cell viability: 28.7 ± 5.4%). These findings indicate that the b-3WJ$^{siEGFR}_{Let\text{-}7g}$ can be efficiently delivered by TrQ*β* VLPs to perform dual-target gene (EGFR and IKK*α*) silencing for further radiotherapy enhancement in GBMs.

In order to ensure that the Q*β* VLPs-based therapeutics prepared the bioproduction process are not toxic to mice, we analyzed the endotoxin concentration in WT-Q*β*. The results showed that the purified WT-Q*β* are almost free of endotoxin (Figure S15). We also investigated the cytotoxicity toward U87MG cells induced by WT-Q*β* (without 3WJ RNAs). No significant inhibition of cell proliferation was observed in the WT-Q*β* treated group (from 0.5 to 4 *μ*M) for 24 h compared

https://doi.org/10.1021/acsnano.3c01102
ACS Nano 2023, 17, 10407−10422

with control group (Figure S16). The overall results indicate that Qβ VLPs-based therapeutics are safe enough to be used in future clinical gene therapy. The promising dual-gene silencing and RNAi distribution monitoring outcomes instigated our exploration into whether TrQβ@b-3WJ$^{siEGFR}_{Let\text{-}7g}$ performed a therapeutic response well to tumors *in vivo*.

Next, we investigated the distribution of the Qβ VLPs-based therapeutics in tumor tissue after CED infusion (Figure 6a and 6b). Both rQβ@b-3WJ$^{siEGFR}_{Let\text{-}7g}$ and TrQβ@b-3WJ$^{siEGFR}_{Let\text{-}7g}$ can penetrate into the tumor tissue from the injection site located at the junction of tumor tissue and normal brain tissue after 0.5 h of CED infusion and reached the maximum dose at 2 h. Moreover, increasingly stronger red fluorescence signals were observed for TrQβ@b-3WJ$^{siEGFR}_{Let\text{-}7g}$ and significantly retained inside tumor tissue for a longer time and have not been eliminated until 24 h after CED infusion, indicating excellent tumor penetrability. Furthermore, b-3WJ$^{siEGFR}_{Let\text{-}7g}$ was taken up in mouse brain tumor cells and was easily monitored without extra tracer labeling after administration of TrQβ@b-3WJ$^{siEGFR}_{Let\text{-}7g}$ by CED using a fluorescence microscope. As shown in Figure S17, the green fluorescence accumulated at the injection site in the mouse brain tumor clearly after administration of TrQβ@b-3WJ$^{siEGFR}_{Let\text{-}7g}$ by CED. Moreover, the delivered b-3WJ$^{siEGFR}_{Let\text{-}7g}$ began to spread from the injection site to surrounding tissues and entered cells 2 h after administration for efficient gene silencing.

The above-mentioned promising *in vitro* outcomes instigated our exploration into whether TrQβ@b-3WJ$^{siEGFR}_{Let\text{-}7g}$ performed well *in vivo*. In the first, we investigated the gene silencing efficiency of rQβ@b-3WJ$^{siEGFR}_{Let\text{-}7g}$ and TrQβ@b-3WJ$^{siEGFR}_{Let\text{-}7g}$ to downregulate the expression of NF-κB by Western blot analysis and immunohistochemistry. The results demonstrated that the concentration of NF-κB in tumor tissue cells can be reduced when the tumor-bearing mice received one dose of rQβ@b-3WJ$^{siEGFR}_{Let\text{-}7g}$, and reduced more when the mice received one dose of TrQβ@b-3WJ$^{siEGFR}_{Let\text{-}7g}$ (Figure S18 and S19). Subsequently, the tumor-bearing mice, through transplantation of U87MG cells into their brains, were infused with 5 μL of carboplatin or rQβ@b-3WJ$^{siEGFR}_{Let\text{-}7g}$ or TrQβ@b-3WJ$^{siEGFR}_{Let\text{-}7g}$ by CED infusion followed by 2Gy X-ray irradiation (Figure 6c). The above course of treatment was repeated after 7 days of initial treatment. Brain magnetic resonance (MR) images were obtained from each animal subgroup to measure the brain tumor volume after various treatments (Figure 6d). The effect of EGFR and IKKα dual-gene silencing and thereby NF-κB downregulation by TrQβ@b-3WJ$^{siEGFR}_{Let\text{-}7g}$ on tumor progression with low-dose X-ray irradiation (2Gy) was analyzed, and the results are presented in Figure 6e and f. The tumor-bearing mice without any treatment (control; 160.5 $\pm$ 44.0 mm^3 on Day 34 and 179.7 $\pm$ 22.8 mm^3 on Day 41) and the mice that received two doses of TrQβ VLPs via CED infusion (141.3 $\pm$ 53.2 mm^3 on Day 34 and 171.3 $\pm$ 40.1 mm^3 on Day 41) all developed large brain tumors in the treated hemisphere, resulting in a median survival time of 27 days and 32 days for the control and TrQβ VLPs-treated groups, respectively. Although the tumor-bearing mice that received two rounds of 2Gy X-ray irradiation or two doses of TrQβ@b-3WJ$^{siEGFR}_{Let\text{-}7g}$ via CED infusion all developed significantly smaller brain tumors (56.0 $\pm$ 22.7 mm^3 for X-ray irradiation only and 67.7 $\pm$ 20.7 mm^3 for TrQβ@b-3WJ$^{siEGFR}_{Let\text{-}7g}$ only on Day 34) than the control and TrQβ VLPs-treated groups, recurrence was observed after 34 days of treatment (127.5 $\pm$ 45.8 mm^3 for X-ray irradiation only and 177.3 $\pm$ 25.7 mm^3 for TrQβ@b-3WJ$^{siEGFR}_{Let\text{-}7g}$ only on Day 41). No obvious improvement in survival rate was observed (median survival = 31 days for both groups) compared with the control and TrQβ VLPs-treated groups by the log-rank analysis (Table S1), indicating that (1) the 2Gy X-ray may not cause enough double-strand breaks (DSBs) and that the cells still process DNA repair to promote tumor cell growth, (2) the TrQβ@b-3WJ$^{siEGFR}_{Let\text{-}7g}$ can only perform gene silencing to inhibit the DNA repair and slow down the tumor cell growth rate, not directly kill tumor cells (Figure S20). Significant tumor growth inhibition was observed (18.9 $\pm$ 17.8 mm^3 on Day 34) compared with the 2Gy X-ray irradiation group when the mice received 5 μL of carboplatin via CED infusion followed by 2Gy X-ray irradiation, most likely because carboplatin is known to sensitize cells to X-rays by enhancing the generation of DSBs and persistent single-strand breaks (SSBs).[41] However, slight recurrence was observed after 34 days of treatment (55.2 $\pm$ 36.5 mm^3 on Day 41), most likely because carboplatin has only the function of enhancing the generation of DSBs without the ability of DNA repair inhibition. Only one of the ten mice (10%) that received CED infusion of two doses of carboplatin at a volume of 5 μL for each followed by 2Gy X-ray irradiation survived over 54 days (median survival = 51 days). Even so, its therapeutic efficiency is still better than that of rQβ@b-3WJ$^{siEGFR}_{Let\text{-}7g}$ enhanced radiotherapy group (median survival = 41 days) due to the relatively low cell penetration efficiency of rQβ@b-3WJ$^{siEGFR}_{Let\text{-}7g}$, which could not efficiently downregulate NF-κB expression to inhibit DNA repair. Noteworthy, the combination of TrQβ@b-3WJ$^{siEGFR}_{Let\text{-}7g}$ pretreatment with 2Gy X-ray irradiation provided nearly complete suppression of tumor progression (8.9 $\pm$ 12.5 mm^3 on Day 41, and no significant tumor recurrence was observed until Day 50 using this gene-silencing-enhanced radiotherapy), which resulted in approximately 50% treated mice surviving over 60 days (median survival = 60 days). Comparing TrQβ@b-3WJ$^{siEGFR}_{Let\text{-}7g}$ + 2Gy X-ray irradiation treatment group with other treatment groups, significant differences ($p < 0.05$) were observed in tumor volume change on Day 41 and in survival using Student's *t* test and log-rank test (Table S1).

The increase in the median survival time (IST$_{median}$; in %) of the X-ray irradiation group was set as the standard baseline (IST$_{median}$ = 100%); the IST$_{median}$ for the mice that received the combination of rQβ@b-3WJ$^{siEGFR}_{Let\text{-}7g}$ pretreatment with 2Gy of X-ray irradiation increased to 132%, indicating that the rQβ@b-3WJ$^{siEGFR}_{Let\text{-}7g}$ can inhibit DNA repair process to enhance the efficiency of radiotherapy. However, it is worth noting that the IST$_{median}$ increased nearly 1.5-fold to 194% when the mice received the combination of TrQβ@b-3WJ$^{siEGFR}_{Let\text{-}7g}$ pretreatment with 2Gy of X-ray irradiation, which means that the TrQβ@b-3WJ$^{siEGFR}_{Let\text{-}7g}$ can enter tumor tissue cells more efficiently compared with rQβ@b-3WJ$^{siEGFR}_{Let\text{-}7g}$, and the therapeutic efficiency of radiotherapy was substantially promoted by TrQβ@b-3WJ$^{siEGFR}_{Let\text{-}7g}$-based gene-silencing-enhanced radiotherapy. Finally, the toxicity of Qβ VLP-based therapeutics (TrQβ VLPs and TrQβ@b-3WJ$^{siSCR}_{MG}$) was evaluated to ensure their safety. Histopathologic examination revealed no obvious differences in the brain tissue sections of the saline, TrQβ VLPs, and TrQβ@b-3WJ$^{siSCR}_{MG}$-treated mice, indicating an absence of neurological toxicity during CED infusion of Qβ VLP-based therapeutics over a 5-day observation period (Figure S21). Our previous blood biochemical analyses showed that the Qβ VLP-based therapeutics would not cause both liver and renal functions, and there were no signs of

https://doi.org/10.1021/acsnano.3c01102
ACS Nano 2023, 17, 10407−10422

inflammation or antigenicity.[23] Additionally, no significant body weight loss was observed in the mice treated with TrQβ VLPs or rQβ@b-3WJ$^{siEGFR}_{Let\text{-}7g}$ or TrQβ@b-3WJ$^{siEGFR}_{Let\text{-}7g}$ (Figure S22). The overall results indicate that TrQβ@b-3WJ$^{siEGFR}_{Let\text{-}7g}$-based genetic therapeutics are efficient and safe enough for use with low-dose X-ray irradiation in future clinical brain tumor treatment modalities.

DISCUSSION

Since GBMs are radioresistant malignancies, most GBM recurrences occur after radiotherapy. Thus, the effectiveness of radiotherapy can be enhanced by target gene-silencing using siRNA or miRNA, which has recently attracted attention. However, the difficulty in precisely tuning the composition and RNA loading in nanoparticles leads to batch-to-batch variations of the RNA drugs, thus significantly restricting their clinical translation. We have developed a biological manufacturing technique to produce bacteriophage Qβ particles with designed 3WJ RNA packaging capable of delivering two different siRNA or miRNA to GBM cells and real-time monitoring RNA cleavage status in cells using fluorescence microscopy. By inserting one siRNA and one miRNA into the 3WJ RNA scaffold, combined with TAT peptide modification on the bacteriophage Qβ particle surface, we obtained a bacteriophage particle, termed TrQβ@b-3WJsiRNA miRNA, with superior cell avidity, efficient multigene silencing, and real-time RNA structural integrity monitoring function in U87MG cells.

For RNAi therapeutics, the stability of RNA in biological condition is an important factor in determining its therapeutic efficiency. The RNA backbones with 2′-fluorine, 2′-*O*-methyl, or 2′-amine modified U and C nucleotides are commonly used to render the RNAs resistant to RNase degradation or hydrolysis so far.[42] However, the chemical process not only affects the biological functions of RNA molecules but also contributes to higher production costs and lower yields. The presented technique in this study has shown that the biological production of 3WJ RNAs followed by immediate self-assembly in bacteriophage particles can greatly protect the RNA molecules from degradation by Rnase. For intracellular RNA distribution monitoring, RNA molecules are usually modified with fluorophores at either their 5′ or 3′ end for intracellular RNA distribution monitoring using fluorescence microscopy, but their further cleavage status with Dicer enzyme cannot be determined.[43] At present, the Northern blotting method is commonly used to analyze the fragments from cleaved RNA by Dicer enzyme in cells, which is very complicated and time-consuming. But now, our designed light-up 3WJ RNA scaffold provides a convenient tool distinct from the Northern blotting for researchers to monitor the cleavage status of delivered RNA molecules with Dicer enzyme in real time by fluorescence microscopy.

To test TrQβ@b-3WJ$^{siRNA}_{miRNA}$, we silenced two genes to downregulate NF-κB expression capable of inhibiting DNA repair after chemotherapy or radiotherapy. One of them, EGFR, promotes the activation of survival signaling pathways. Increased EGFR activation and overexpression is strongly associated with tumorigenesis, tumor progression, and tumor invasion.[44] Recently, it has been reported that nuclear translocation of EGFR also promotes the repair of DSBs after IR. The possible mechanism is that the downregulation of EGFR inhibits the expression of the IKK complex and thereby inactivates NF-κB signaling to inhibit DNA repair,[38] but it remains to be determined in detail. Our second target, IKKα, forms the catalytic subunit with IKKβ to regulate subunit IKKγ thereby promoting IKK complex production. The IKK complex is a central regulator of NF-κB activation. Let-7g, a miRNA, has been reported to directly knock down MEKK1, IKKα and ablates IKKα phosphorylation.[45] Thus, we incorporate one EGFR siRNA sequence and one Let-7g sequence into the 3WJ RNA scaffold to obtain TrQβ@b-3WJ$^{siEGFR}_{Let\text{-}7g}$. We found that silencing those proteins of EGFR and IKKα, using TrQβ@b-3WJ$^{siEGFR}_{Let\text{-}7g}$ enabled RNAi, reduced overall NF-κB expression and activity in the nucleus resulting in a suppression of DNA repair after radiotherapy. Our *in vivo* data provide a proof of principle that the designed 3WJ RNA enables to simultaneously block different signaling pathways of DNA repair mechanisms to enhance cellular response to X-ray irradiation thereby eradicating the tumor of GBMs and suppressing tumor recurrence. Owing to the modular character of b-3WJ RNA scaffold, this approach can be adapted for silencing any other genes (i.e., Akt, Bcl-xL, VEGF, TNFα, STAT3, etc.) by inserting different target sequences of siRNA/miRNA into b-3WJ RNA scaffold, which enables containing three different target sequences for multigene silencing. The technology we describe here is suitable for rapidly testing the function of highly expressed genes and drug candidates *in vivo*.

CONCLUSIONS

In summary, we have successfully developed TrQβ@b-3WJ$^{siEGFR}_{Let\text{-}7g}$-based genetic therapeutics, which can efficiently knock down EGFR and IKKα simultaneously and inactivate NF-κB signaling, thereby inhibiting DNA repair in a highly efficient manner for enhancing radiotherapy. Impressively, the status of released b-3WJ$^{siEGFR}_{Let\text{-}7g}$ processed into its mature form by Dicer for gene silencing can be easily and real-time monitored using fluorescence microscopy. TrQβ@b-3WJ$^{siEGFR}_{Let\text{-}7g}$ showed a robust ability to protect packaged RNA scaffolds from unwanted threats (i.e., enzymatic digestion), high tumor cell penetration efficiency, and surrounded the whole tumor with a high concentration of b-3WJ$^{siEGFR}_{Let\text{-}7g}$ by CED infusion, which can bypass the blood-brain barrier BBB to reduce systemic toxicity. Conspicuously, these genetic therapeutics provide a chance to serve as a powerful gene-silencing-enhanced radiotherapy for clinical GBM treatment and other brain diseases of the central nervous system.

MATERIALS AND METHODS

Plasmid Construction for Qβ VLPs and 3WJ RNA Scaffolds. The QβCP expression vector pCDF-QβCP was constructed according to our previous study.[46] The QβCP DNA sequence and mCherry red fluorescent protein DNA sequence were inserted into the pCDFDuet-1 plasmid. The mCherry DNA sequence was originally from plasmid pmCherry. After cloning into the pET28-b(+) plasmid using *Bam*HI and NotI restriction enzymes for insertion, the mCherry sequence was cloned into pCDFDuet-1 to produce the plasmid pCDFDuet-1-mCherry. The QβCP sequence was originally from pCDFDuet-1-QβCP-GFP, which has been described previously[26] and was inserted into the pCDFDuet-1-mCherry plasmid using EcoNI and the XhoI restriction site to produce the protein expression vector pCDFDuet-1-QβCP-mCherry.

The multifunctional 3WJ RNA scaffold gene sequence was purchased from GENEWIZ and cloned into the pET28-b(+) plasmid using the *Bgl*II and XhoI restriction sites to produce the RNA scaffold expression vector pET28-b(+)-3WJ. The primers used in this study are listed in the table below.

https://doi.org/10.1021/acsnano.3c01102
ACS Nano 2023, 17, 10407−10422

Table 1

Primer ID	Sequence (5′-3′)
Qβ_FWD	GTGGGAATTCCATGGCAAAATTAGAGACTGT
Qβ_REV	CACCAAGCTTTCAATACGCTGGG
T7_FWD	GTGGAGATCTTAATACGACTCACTATAGGGCCAT
T7_REV	CACCCTCGAGCAAAAAACCCCTCAAGACCC

Bioproduction of 3WJ Scaffold Packaging VLPs. The vectors pCDF-QβCP (stp^R) and pET28-b(+)-3WJ (Kan^R) were transformed into *E. coli* strain BL21 (HIT-21, RBC, USA) to produce 3 WJ scaffolds packaged in VLPs without fluorescent protein (Qβ@b-3WJ).

For coexpression of QβCP, mCherry protein and the 3 WJ RNA scaffold, pCDFDuet-1-QβCP-mCherry (stp^R) and pET28-b(+)-3WJ (Kan^R) were transformed into *E. coli* BL21 cells (HIT-21, RBC, USA) for expression. *E. coli* BL21 cells harboring the plasmids were grown in either LB broth supplemented with antibiotic (streptomycin) at 50 μg/mL. Starter cultures were grown for 18 h at 37 °C and were used to inoculate 1 L of expression culture. IPTG (1 nM) was used as a protein expression reagent at an $OD_{600\ nm}$ of 0.8−1.0 in LB broth. The IPTG-supplemented culture was incubated at 37 °C overnight for approximately 16−18 h. The overnight culture was harvested by centrifugation at 6500*g*, resuspended in 20 mL of PBS buffer (pH = 7.4) and then lysed by sonication. The lysate was centrifuged for 30 min at 23000*g*, followed by ammonium sulfate precipitation, which was used to obtain crude VLPs. Crude VLPs were resuspended in PBS buffer, followed by 20% w/v PEG8000-NaCl precipitation to obtain pure VLPs. VLPs were resuspended in 1 mL PBS buffer and extracted with 1:1 *n*-butanol:chloroform. The VLP-based samples from the aqueous layer were purified by step sucrose gradient ultracentrifugation and then precipitated with 20% w/v PEG8000/2 M NaCl solution and resuspended in 25 mL of PBS buffer, followed by exhaustive dialysis (SnakeSkin Dialysis Tubing, 10,000 MWCO. Thermo, LOT: QD213952, USA) against PBS buffer (pH = 7.4) for 48 h. The obtained pure VLP-based samples were concentrated using protein concentrate filter tubes (Amicon Ultra15 Centrifugal Filter Units. 100,000 MWCO. Merck Millipore, LOT: R6EA45140, Ireland). The final concentration of VLPs was assessed using a Pierce BCA Protein Assay kit (Thermo, LOT: PD202250, USA).

TAT-Peptide Conjugation Procedure and Analysis. The functional peptide cys-TAT was conjugated on the surface of rQβ@b-3WJ to enhance cell uptake.[23] The Cys-TAT peptides (KYGRRRQRRKKRG-cys-SH) were conjugated to rQβ@b-3WJ by sulfosuccinimidyl 4-(N-maleimidomethyl) cyclohexane-1carboxylate (sulfo-SMCC; Sigma-Aldrich, St. Louis, MO, USA) as a cross-linker. Briefly, 5 μL of sulfo-SMCC solution (10 mg/mL in deionized (DI)-H_2O) was added to a 600 μL solution of 2 μM rQβ@b-3WJ in PBS buffer (pH = 7.4) for 30 min at 25 °C in the dark and then purified using a filter column (Amicon Ultra15 Centrifugal Filter Units. 100,000 MWCO. Merck Millipore, LOT: R6EA45140, Ireland) with PBS buffer. The samples were desalted with a filter column (100,000 MWCO) and washed 3 times with PBS buffer. Subsequently, the maleimide-terminated rQβ@b-3WJ was reacted with 30 μL of Cys-TAT solution (0.3 mg/mL) at 25 °C for 2 h in the dark and then purified again using the above-mentioned procedure to obtain TrQβ@b-3WJ.

To confirm the successful conjugation of TAT peptides on Qβ@b-$3WJ^{siEGFR}_{siLUC}$. The Qβ@b-$3WJ^{siEGFR}_{siLUC}$ and TQβ@b-$3WJ^{siEGFR}_{siLUC}$ were mixed with 2-mercaptoethanol (SigmaAldrich, St. Louis, MO, USA) and incubated at 95 °C for disulfide bond breaking and protein denaturing. The denatured samples were analyzed by SDS-PAGE (12%) electrophoresis and then stained using Coomassie Brilliant Blue R-250 Dye (Sigma−Aldrich, St. Louis, MO, USA).

Dynamic Light Scattering Characterization. The diameters of VLP-based samples in PBS buffer (pH = 7.4) were analyzed by dynamic light scattering (DLS). Two hundred microliters of the VLP-based sample (Qβ VLPs and Qβ@b-$3WJ^{siSCR}_{MG}$) solution was added to a 3-open microvolume cuvette for diameter analysis.

Transmission Electron Microscopy (TEM). Five microliters of VLP-based samples were pipetted onto Formvar-coated copper mesh grids (400 mesh, Ted Pella, Redding, CA, USA) for 5 min, followed by exposure to 8 μL of a solution of uranyl acetate (15 mg/mL in DI-H_2O) for 2 min as a negative stain. Excess stain was then removed, and the grids could dry in air for 10 min.

In-Gel Urea Page Electrophoresis of RNA Scaffolds. *In vitro* transcribed b-3WJ RNA scaffolds were prepared following the protocol of the HiScribe T7 High Yield RNA Synthesis Kit (NEB, USA). The packaged b-3WJ RNA scaffolds were prepared by extracting the b-3WJ RNA scaffolds from Qβ@b-3WJ according to our previously described methods.[26,32] Purified RNAs (1 μg/well) were electrophoresced with 8% urea page at 90 V for 4 h. After washing with DI-H_2O, the gel was stained with DFHBI-1T to observe the broccoli aptamer, followed by SYBR green II staining to observe the total RNA.

RNA Scaffold Fluorescence Assay. Purified Qβ@b-3WJ was resuspended in RNA aptamer binding buffer (40 mM 4-(2-hydroxyethyl)-1-piperazineethanesulfonic acid) HEPES, 100 mM KCl, 1 mM $MgCl_2$, pH = 7.4), coincubated with 10 μM DFHBI-1T for 30 min at 37 °C and subjected to UV−vis spectrometry to measure the maximum absorbance wavelength as the fluorescence excitation wavelength. Fluorescence intensity measurement was performed using an M2 enzyme-linked immunosorbent assay (ELISA) spectrometer (Molecular Device, Silicon Valley, CA, USA).

Stability Studies of the b-3WJ RNA Scaffold Packaged in Qβ VLPs. *In vitro* transcribed b-3WJ RNA scaffolds were produced by the method mentioned previously using the HiScribe T7 High Yield RNA Synthesis Kit (NEB, USA).[26] Approximately 1 μM naked b-3WJ RNA or 1 μM packaged b-3WJ RNA was pretreated with 10 μM DFHBI-1T in RNA binding buffer and incubated at 37 °C for 30 min followed by mixing with various concentrations of Rnase A. The fluorescence intensity (E_x = 418 nm, E_m = 510 nm) was then analyzed using an M2 ELISA spectrometer to estimate the stability of naked b-3WJ RNA and packaged b-3WJ RNA at different time points.

We also investigated the stability of naked b-3WJ RNA and packaged b-3WJ RNA after treatment with 10 mg/mL urea for 0, 1, 2, 4, 15, 24, 48, 72, 96, 120, and 144 h. Then, the fluorescence intensity was analyzed to estimate the stability of naked b-3WJ RNA and packaged b-3WJ RNA at different time points by an M2 ELISA spectrometer.

***In Vitro* Cell Culture.** The glioma cell Line U87MG was cultured in Dulbecco's modified Eagle's medium (DMEM) supplemented with 2.2 mg/mL sodium carbonate, 10% fetal bovine serum (FBS), 50 μg/mL gentamicin, 50 μg/mL penicillin, and 50 μg/mL streptomycin. Cells were harvested by 0.05% trypsin-ethyldiaminetetraacetic acid (EDTA) solution and washed with PBS buffer (pH = 7.4) three times before seeding into experimental wells.

Cell Uptake of VLP-Based Samples by U87MG Tumor Spheroids. U87MG cells were cultured at 5×10^4 cells per well in U-end 96-well plates for 72 h to form a spheroid 3D culture. One micromolar VLP-based samples (rQβ@b-$3WJ^{siEGFR}_{siLUC}$ or TrQβ@b-$3WJ^{siEGFR}_{siLUC}$) were added to the cells and incubated for another 24 h. The cell nuclei were stained with Hoechst 33342, and the b-3WJ RNA scaffolds were stained with DFHBI-1T followed by PBS wash. The distribution of Qβ VLPs and delivered b-$3WJ^{siEGFR}_{siLUC}$ were monitored using laser scanning confocal microscopy.

Broccoli Aptamer Tracking Images in Live Cells. U87MG cells were seeded in a glass-based chamber (~1×10^5 cells per well) and incubated for 24 h. TrQβ@b-$3WJ^{siEGFR}_{siLUC}$ (1 μM) was then added and incubated for another 24 h. The medium was removed, and the cells were washed with PBS followed by incubation with DFHBI-1T-containing medium. The cells were imaged using 3D-Cell Explorer-Fluo microscopy (Nanolive) at 60×, and images were taken every 10 min for cell nuclei (blue color), Qβ VLPs (red color), and b-3WJ RNA scaffolds (green color). The images were merged and analyzed using STEVE Microscopy software (NanoLive).

Northern Blot Analysis. U87MG cells were seeded in 12-well plates (~1×10^5 cells per well) and incubated for 24 h. The TrQβ VLPs (1 μM) or TrQβ@b-$3WJ^{siEGFR}_{siLUC}$ (1 μM) were then added to the

https://doi.org/10.1021/acsnano.3c01102
ACS Nano 2023, 17, 10407−10422

culture medium. The cells were harvested after 24, 26, 36, and 48 h of incubation, and the small RNAs were extracted with the mirVana PARIS kit (Life Technologies, Carlsbad, CA, USA), resolved by denaturing gel electrophoresis (urea PAGE), transferred to a Hybond-N+ membrane (GE Healthcare) by the capillary method and immobilized by UV transillumination (320 nm). Northern blotting was performed according to the manufacturer's protocols (North2-South Chemiluminescent Hybridization and Detection Kit, Thermo Scientific, USA). The membrane was probed with a biotin-labeled DNA oligonucleotide (5′- GCA CAA AGT GTG TAA CGG AAT ACC [Biotin]-3′, high performance liquid chromatography (HPLC) purified, Mission Bio, Inc. Taiwan), which is complementary to the EGFR siRNA. The blotting images were analyzed using ImageJ software to quantify the different length fragments of the RNAs.

Western Blot Analysis. For *in vitro* Western blotting, U87MG cells (6×10^4 per well) in 6-well plates treated with 1 μM VLP-based samples (TrQβ VLPs, TrQβ@b-3WJ$^{siEGFR}_{siLUC}$, rQβ@b-3WJ$^{siEGFR}_{Let\text{-}7g}$, and TrQ$\beta$@b-3WJ$^{siEGFR}_{Let\text{-}7g}$) were harvested and washed with PBS (pH = 7.4). The cells were treated with PRO−PREP Protein Extraction Solution (iNtRON) to extract proteins, and the protein concentration was quantified using a Pierce bicinchoninic acid (BCA) Protein Assay Kit (Thermo). Proteins were electrophoresced using an 8% SDS-PAGE gel (approximately 20 μg per lane) and transferred to a polyvinylidene fluoride (PVDF) membrane. After blocking with blocking solution (5% milk, 0.1% Tween-20 in TBS buffer, pH = 7.4), the beta-actin internal control was stained with beta-actin monoclonal antibody (CAT: 66009−1-Ig, Proteintech, 1/10000 dilution), glyceraldehyde-3-phosphate dehydrogenase (GAPDH) was stained with antiGAPDH antibody (clone 2D9. CAT: TA802519, Invitrogen, 1/5000 dilution). Target protein EGFR was stained with EGFR antibody [GT133] (CAT: GTX628887, GeneTex, 1/2500 dilution), NF-κB (P65) was stained with NF-κB p65/RelA antibody (CAT: A19653, Abclonal, 1/1000 dilution), and luciferase was stained with antifirefly luciferase antibody [Luci17] (ab16466, Abcam, 1/1000 dilution). A goat antimouse IgG (H+L)-HRP antibody was used as the secondary antibody for all proteins mentioned. Chemiluminescence signals were imaged using a ChemiDocTM XRS imaging system.

For *in vivo* Western blotting, the brain tumor tissues of mice treated with 5 μM rQβ@b-3WJ$^{siEGFR}_{Let\text{-}7g}$ or TrQβ@b-3WJ$^{siEGFR}_{Let\text{-}7g}$ were cut into small pieces and carefully washed in 3 mL PBS, then homogenized on ice by a Polytron blender in lysis buffer supplemented with a protease-inhibitor cocktail. The homogenates were centrifuged at 2000 rpm for 10 min at 4 °C, and the supernatant was assayed for total protein concentration by BCA Protein Assay Kit and stored at −80 °C until NF-κB analysis using Western blotting was performed as described above.

Luciferase Reporter Assay. Luciferase-stable U87MG cells treated with 1 μM VLP-based samples (WT-Qβ and TrQβ@b-3WJ$^{siEGFR}_{siLUC}$) for 72 h were harvested and washed with PBS (pH = 7.4). The luciferase expression analysis process of luciferase-stable U87MG cells generally followed the Luciferase RGA high sensitivity, 200 assays (Roche) protocol. The chemiluminescence was detected by an M2 ELISA spectrometer.

Flow Cytometry Analysis. U87MG cells (6×10^4 per well) in 6-well plates were treated with 1 μM VLP-based samples (TrQβ VLPs, rQβ@b-3WJ$^{siEGFR}_{Let\text{-}7g}$, and TrQ$\beta$@b-3WJ$^{siEGFR}_{Let\text{-}7g}$) for 72 h were washed three times with 2% FBS contained PBS (pH = 7.4). After that, all samples were fixed by 4% paraformaldehyde for 15 min and permeabilized by 0.1% triton X-100 solution for 15 min, the cells were separated into three groups (10^5 cells/mL for each). Then, those cells were blocked by 1% BSA solution for 20 min, followed by incubation with EGFR antibody (1/1000 dilution, EGFR Rabbit Ab, CAT: A11351, ABClonal), IKKα antibody (1/1000 dilution, IKKα Rabbit mAb, CAT:A19694, ABClonal), or NF-κB antibody (1/1000 dilution, NF-κB p65/RelA Rabbit mAb, CAT: A19653, ABClonal) for 1.5 h. The cells were further incubated with secondary antibody (1/500 dilution, 488-conjugated Goat Anti-Rabbit IgG (H+L), CAT: AS053, ABClonal) for 1 h. All samples were quantified by Atune Nxt flow cytometer (Thermo Fisher Scientific, USA).

Immunofluorescence Microscopy. U87MG cells (3×10^4 per well in a 24-well plate) were treated with 1 μM VLP-based samples (TrQβ VLPs, rQβ@b-3WJ$^{siEGFR}_{Let\text{-}7g}$, and TrQ$\beta$@b-3WJ$^{siEGFR}_{Let\text{-}7g}$) for 72 h. Then, the cells were washed with PBS (pH = 7.4) and fixed with 75% ethanol. Then, the cells were incubated in blocking solution (10% bovine serum albumin (BSA), 0.3 M glycine and 0.1% Tween-20 in PBS buffer, pH = 7.4) for 1 h. The blocked cells were incubated with EGFR antibody (ab8465, 1/1000 dilution) overnight at 4 °C. The cells were further incubated with goat antimouse IgG (H+L)-FITC secondary antibody (1/1000 dilution). The nuclei were stained using Hoechst 33342, and images were taken using fluorescence microscopy.

***In Vitro* Cell Studies.** The cultured U87MG cells (5,000 cells/well) were treated with Qβ VLPs with final concentrations of 0.5, 1.0, 2.0, and 4.0 μM followed by incubation for 24 h to verify the cytotoxicity of Qβ VLPs. The culture medium was removed, and the cells were incubated in 120 μL of XTT solution for 2 h. After that, 100 μL of XTT solution from each well was transferred to another 96-well counting plate. The survival of U87MG cells was evaluated by OD at 490 nm using a SpectraMax M2 microtiter plate reader.

U87MG cells were treated with 1 μM of VLP-based samples (WT-Qβ, rQβ@b-3WJ$^{siEGFR}_{Let\text{-}7g}$, and TrQ$\beta$@b-3WJ$^{siEGFR}_{Let\text{-}7g}$) for 72 h and then seeded into 96-well plates (1000 cells per well). After 72 h of incubation, the cells were washed with PBS buffer (pH = 7.4) and incubated with XTT solution at 37 °C for 30 min (n = 8). Cell growth rate was analyzed by measuring the absorbance at 450 nm using an SpectraMax M2 microtiter plate reader.

To investigate the *in vitro* synergistic effect of EGFR/IKKα gene silencing and X-ray irradiation, U87MG cells (5,000 cells per well) were treated with 1 μM of TrQβ@b-3WJ$^{siEGFR}_{Let\text{-}7g}$ for 72 h followed by 2Gy X-ray irradiation. After 24 h, the cells were washed with PBS buffer (pH = 7.4) and incubated with XTT solution at 37 °C for 30 min (n = 8). Cell viability was analyzed by measuring the absorbance at 450 nm using an SpectraMax M2 microtiter plate reader. Cell viability (%) was defined as the relative absorbance of the treated samples versus that of the untreated controls.

Transwell Migration Assay. Transwell assays generally followed the Cell Migration, Chemotaxis and Invasion Assay using the Staining protocol (Corning, NY, USA). U87MG cells were treated with VLP-based samples (TrQβ VLPs, rQβ@b-3WJ$^{siEGFR}_{Let\text{-}7g}$, and TrQ$\beta$@b-3WJ$^{siEGFR}_{Let\text{-}7g}$) for 72 h. Then, the treated cells were harvested, resuspended in FBS-free DMEM, and seeded at 2×10^4 cells in the inset of a 24-well Transwell plate. The reservoir volume was 0.65 mL of DMEM containing 10% FBS in each well. After 4 h of incubation, the interior of the Transwell membrane was wiped, and the migrated cells were stained with Giemsa stain and imaged with microscopy.

Endotoxin Assay. Briefly, 100 μL of 2-Mercaptoethanol (20 mM) was mixed with 100 μL of Qβ VLPs (10 μM) or 100 μL of endotoxin standard (100 EU/mL; Endotoxin, *E. coli* O55:B5, cat: 193783) at 37 °C for 30 min followed by filtration using Amicon Ultra-0.5 Centrifugal Filter Unit (UFC5003, Millipore, USA). Then the endotoxin concentration in the elutriant (from Qβ VLPs or endotoxin standard) was then analyzed by Kinetic-QCL Kinetic Chromogenic LAL Assay Kit.

Animal Procedures. For the animal experiments, luciferase expression plasmid-transfected U87MG cell-implanted pathogen-free male NU/NU mice (5−7 weeks old, 20−25 g, from BioLASCO, Taiwan) were employed in this study. U87MG cells were cultured at 37 °C with 5% CO_2 in MEM with 10% fetal bovine serum and 1% penicillin/streptomycin (Invitrogen). Mice were anaesthetized with 2% isoflurane gas and immobilized on a stereotactic frame to implant U87MG cells. A sagittal incision in the skin overlying the calvarium was created. U87MG cell implantation was performed by creating a hole in the exposed cranium 1.5 mm anterior and 2 mm lateral to the bregma using a 27G needle. A total volume of 5 μL of U87MG cell suspension (1×10^5 cell/μL) was injected at a depth of 3 mm from the brain surface over a 5 min period. The needle was withdrawn over 2 min. MRI was performed to monitor brain tumor growth for 7 days after tumor cell implantation.

https://doi.org/10.1021/acsnano.3c01102
ACS Nano 2023, 17, 10407−10422

CED Procedures. The details of the CED procedure are as described in our previous study. Briefly, infusion cannulas were fabricated with silica tubing (Polymicro Technologies, Phoenix, AZ, USA) fused to a 0.1 mL syringe (Plastic One, Roanoke, VA, USA) with a 0.5 mm stepped-tip needle that protruded from the silica guide base. The treatment agents (VLPs or drugs) were loaded into the syringes and attached to a microinfusion pump (Bioanalytical Systems, Lafayette, IN, USA). The syringe with a silica cannula was mounted onto a stereotactic holder and then lowered through a puncture hole made in the skull to the implanted tumor. The sample solution was infused at a rate of 1 μL/min until a volume of 5 μL had been delivered, and the cannula was removed 2 min later.

***In Vivo* Antitumor Efficiency of Gene Silencing-Enhanced Radiotherapy.** All animal experiments were approved by the Animal Committee of Chang Gung University and adhered to the experimental animal care guidelines (IACUC NO. CGU106-036). Mice were raised in a room with a thermostat at 26 °C. Nu/Nu mice weighing approximately 25−30 g (5−6 weeks old) were tested to confirm the efficacy of the proposed approach. Intracranial brain tumors were induced by transplantation of U87MG cells into mouse brains. Briefly, cultured U87MG cells (5×10^5 cells/mouse) were injected over a 2 min period into the brain using a syringe, and needle withdrawal was conducted over another period of 0.5 min. A total of 50 mice were used, and the experiments were divided into five groups. In Group 1 (n = 10), the mice received no further treatment after transplantation of U87MG cells, and these mice served as the control. In Group 2 (n = 10), the mice received TrQβ VLPs (5 μM) via CED infusion two times (every 7 days) after 7 days of U87MG cell transplantation. In Group 3 (n = 10), the mice received X-ray irradiation (2Gy) two times (every 7 days) after 7 days of U87MG cell transplantation. In Group 4 (n = 10), the mice received carboplatin (10 mg/mL) via CED infusion at 9 A.M. followed by 2Gy X-ray irradiation at 2 P.M. the following day. Seven days after U87MG cell transplantation, the treatment was repeated two times (every 7 days). In Group 5 (n = 10), the mice received TrQβ@b-3WJ$^{siEGFR}_{Let\text{-}7g}$ (5 μM) via CED infusion at 9 A.M. Seven days after U87MG cell transplantation, the treatment was repeated two times (every 7 days). In Group 6 (n = 10), the mice received rQβ@b-3WJ$^{siEGFR}_{Let\text{-}7g}$ (5 μM) via CED infusion at 9 A.M. followed by 2Gy X-ray irradiation at 2 P.M. the following day. Seven days after U87MG cell transplantation, the treatment was repeated two times (every 7 days). In Group 7 (n = 10), the mice received TrQβ@b-3WJ$^{siEGFR}_{Let\text{-}7g}$ (5 μM) via CED infusion at 9 A.M. followed by 2Gy X-ray irradiation at 2 P.M. the following day. Seven days after U87MG cell transplantation, the treatment was repeated two times (every 7 days). The intracranial tumor volume in mice was measured by MR imaging. The survival time was calculated from the day of U87MG cell inoculation (0 day) to the day of death. Kaplan−Meier survival curves were plotted for each group. The body weight of the mice was monitored at determined time intervals.

Histopathological Studies. Histopathological studies were performed on 10-μm sections of paraformaldehyde-fixed, paraffin-embedded mouse brains. Slides were soaked in hydrochloric acid−potassium ferrocyanide solution for 30 min at room temperature. The distribution of delivered b-3WJ$^{siEGFR}_{Let\text{-}7g}$ conjugated with DFHBI-1T (green fluorescence) was monitored through fluorescence microscopy imaging after staining nuclei with DAPI. The images were taken after 0.5, 1, and 2 h of CED infusion. For brain tissue damaging situation evaluation, brain tissues from the mice after 5 days of different treatments [5 μL of saline, 5 μL of TrQβ VLPs (5 μM), and 5 μL of TrQβ@b-3WJ$^{siSCR}_{MG}$ (5 μM)] were stained by hematoxylin and eosin (H&E).

Statistical Analysis. The data were expressed as the mean ± SD on the basis of at least three independent experiments. Statistical analysis was performed using Student's *t*-test and log-rank test. Differences were considered statistically significant if $p < 0.05$.

ASSOCIATED CONTENT

Supporting Information

The Supporting Information is available free of charge at https://pubs.acs.org/doi/10.1021/acsnano.3c01102.

Supplementary Figures (S1− S22) and Table S1, including detailed gene silencing mechanisms of TrQβ@b-3WJ$^{siEGFR}_{Let\text{-}7g}$ toward GBM cells, design of the dual-plasmid coexpression production system of the b-3WJ RNAi scaffold containing Qβ VLPs in this project, dynamic light scattering (DLS) of WT-Qβ and Qβ@b-3WJ$^{siSCR}_{MG}$, calibration curve of the b-3WJ RNA scaffold with DFHBI-1T coincubation to quantify the number of RNAi scaffolds for each Qβ VLP, fluorescence spectra of VLP-based samples, stability studies of b-3WJ RNAs, Western blotting of EGFR expression, fluorescence spectra and image of TrQβ@b-3WJ$^{siEGFR}_{Let\text{-}7g}$, stability of TrQ$\beta$@b-3WJ$^{siEGFR}_{Let\text{-}7g}$ in RNase A, flow cytometry analysis of EGFR, IKKα, and NF-κB expression after treatment, wound healing assay, trans-well assay, cell growth assay, *in vitro* synergistic effect of EGFR/IKKα gene silencing and X-ray irradiation, endotoxin assay of purified WT-Qβ, cell viability of U87MG cells treated with WT-Qβ, distribution of delivered b-3WJ$^{siEGFR}_{Let\text{-}7g}$ after CED infusion, Western blotting of NF-κB (P65) expression in tumor tissue, inhibition of NF-κB (P65) by gene silencing therapy, tumor volume measurement by MRI, brain damage and toxicity evaluation using H&E staining, body weight of mice that received different treatments, and Log-rank analysis result of survival study (PDF)

AUTHOR INFORMATION

Corresponding Authors

Kuo-Chen Wei − *Department of Neurosurgery, Neuroscience Research Center, Chang Gung Memorial Hospital, Linkou, Taoyuan 33305, Taiwan; School of Medicine, Chang Gung University, Taoyuan 33302, Taiwan; Department of Neurosurgery, New Taipei Municipal TuCheng Hospital, New Taipei City 23652, Taiwan*; Email: kuochenwei@cgmh.org.tw

Hung-Wei Yang − *Department of Biomedical Engineering, National Cheng Kung University, Tainan 70101, Taiwan; Medical Device Innovation Center, National Cheng Kung University, Tainan 70101, Taiwan*; orcid.org/0000-0002-8438-6291; Email: howardyang@gs.ncku.edu.tw

Authors

Hao-Han Pang − *Department of Biomedical Engineering, National Cheng Kung University, Tainan 70101, Taiwan*; orcid.org/0000-0001-9071-9649

Chiung-Yin Huang − *Department of Neurosurgery, Neuroscience Research Center, Chang Gung Memorial Hospital, Linkou, Taoyuan 33305, Taiwan*

Pin-Yuan Chen − *Department of Neurosurgery, Neuroscience Research Center, Chang Gung Memorial Hospital, Linkou, Taoyuan 33305, Taiwan; School of Medicine, Chang Gung University, Taoyuan 33302, Taiwan; Department of Neurosurgery, Chang Gung Memorial Hospital, Keelung, Keelung 20401, Taiwan*

Nan-Si Li − *Department of Biomedical Engineering, National Cheng Kung University, Tainan 70101, Taiwan*; orcid.org/0000-0002-6991-6223

https://doi.org/10.1021/acsnano.3c01102
ACS Nano 2023, 17, 10407−10422

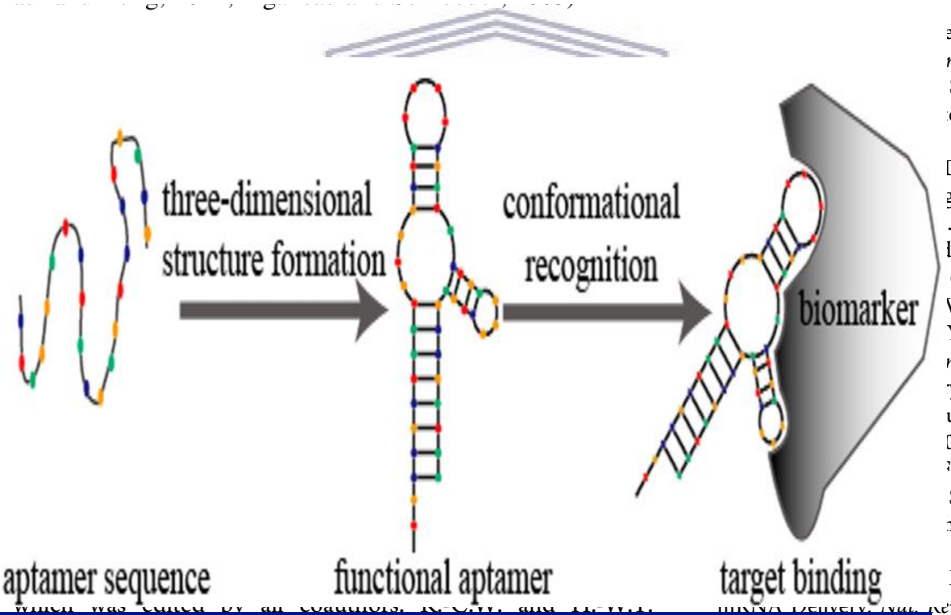

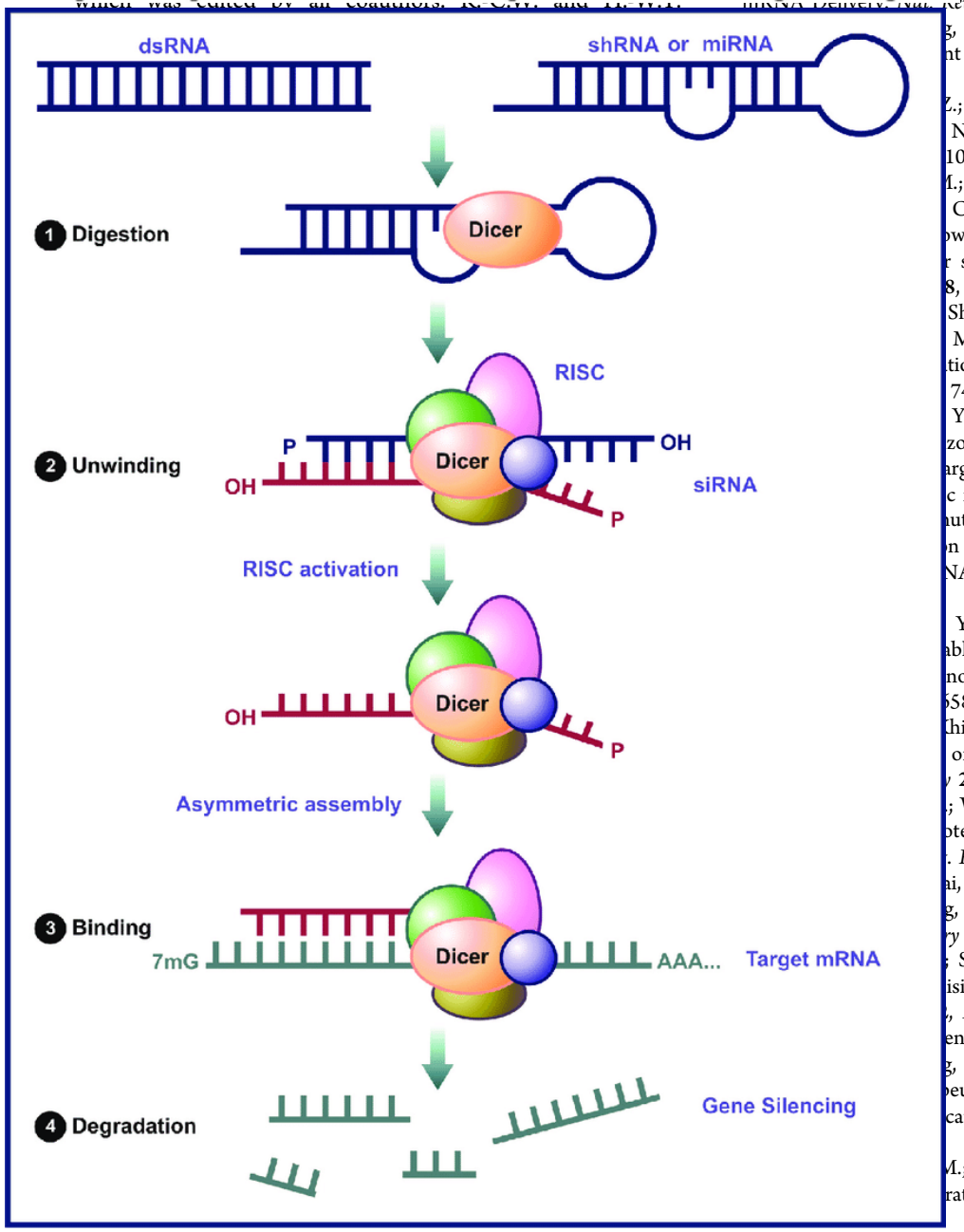

e by Preferential Activation of the DNA
re **2006**, *444*, 756−760.
S. C.; Mulkearns-Hubert, E. E.; Valentim, C.
em Cells in Glioblastoma. *Genes Dev.* **2015**,

D.; Kawaguchi, R.; Nair, P.; Prasad, R.; Qin,
g, Q.; VanderVeer-Harris, N.; Pham, A.;
. P300 Promotes Tumor Recurrence by
luced Conversion of Glioma Stem Cells to
Commun. **2022**, *13*, 6202. Wang, J.; Cazzato,
V.; Rosenbloom, D. I. S.; Zairis, S.; Abate, F.;
Y. J.; et al. Clonal Evolution of Glioblastoma
net. **2016**, *48*, 768−776.
y, T. E.; Bressler, L. R. Temozolomide in
urrent Use and Future Targets. *Cancer*
009, *64*, 647−655.
.; Hallahan, B.; Reif, R.; Li, H. Uniqueness,
Solutions, and Perspectives in Therapeutics
nology. *Nucleic Acid Ther.* **2012**, *22*, 226−

Langer, R.; Dong, Y. Lipid Nanoparticles for
ev. Mater. **2021**, *6*, 1078−1094.
g, S.; Lv, J.; Cheng, Y. Design of Polymers for
nt Progress and Challenges. *VIEW* **2021**, *2*,

Z.; Saha, K.; Kim, C. S.; Kim, S. T.; Landis, R.
Nanoparticles for Nucleic Acid Delivery. *Mol.*
1083.
M.; Wang, J. T.; Faruqu, F. N.; Benitez, J.;
C.; Kondo, A.; Al-Jamal, K. T. Engineering
owth Receptor 2-Targeting Hepatitis B Virus
r siRNA Delivery *in Vitro* and *in Vivo*. *ACS*
8, *1*, 3269−3282.
Sharma, A.; Rajabi, M.; Haque, F.; Shu, D.;
M.; Guo, P. Stable RNA Nanoparticles as
tion Drugs for Cancer Therapy. *Adv. Drug*
74−89.
Y.; Shu, D.; Li, H.; Zhang, J.; Yu, J. G.; Jaime-
zo, M.; Romano, G.; Cui, R.; et al. RNA
rgeted Therapy for Glioblastoma through
c miR-21. *Mol. Ther.* **2017**, *25*, 1544−1555.
utdinov, E. F.; Zhang, L.; Guo, P. Program-
n RNA *in Vivo* and *in Vitro* Driven by pRNA
NA Packaging Motor. *Nucleic Acids Res.* **2014**,

Y.; Haque, F.; Abdelmawla, S.; Guo, P.
able RNA Three-Way Junction for Construct-
noparticles for Delivery of Therapeutics. *Nat.*
58−667.
hisamutdinov, E. F.; Guo, P. Entropy-Driven
of Phi29 pRNA 3WJ from Three RNA
2014, *53*, 2221−2231.
; Wang, Y.; Liu, J.; Duan, D. Advancements in
otechnology and Its Application for Cancer
. *Front. Biosci. (Landmark Ed.)* **2022**, *27*, 61.
ai, H.; Steinmetz, N. F. Viral Nanoparticles for
g, Immunotherapy, and Theranostic Applica-
ry *Rev.* **2020**, *156*, 214−235.
; Samy, W. M.; Elgindy, N. A. Protein-Based
ising Drug and Gene Delivery Systems. *J.*
, *161*, 38−49.
en, P. Y.; Wei, K. C.; Huang, C. W.; Shiue, Y.
g, H. W. Convection-Enhanced Delivery of a
eutic Agent with Dual-Modal Imaging for
cation of Brain Tumors. *Theranostics* **2019**, *9*,

M.; Shi, H.; Gao, S.; Xie, G.; Zhu, M.; Wu, M.;
ration of Cell-Penetrating Peptides with Rod-

https://doi.org/10.1021/acsnano.3c01102
ACS Nano 2023, 17, 10407−10422

like Bionanoparticles: Virus-Inspired Gene-Silencing Technology. *Nano Lett.* **2018**, *18*, 5453−5460.
(25) Lam, P.; Steinmetz, N. F. Delivery of siRNA Therapeutics Using Cowpea Chlorotic Mottle Virus-Like Particles. *Biomater. Sci.* **2019**, *7*, 3138−3142.
(26) Pang, H. H.; Huang, C. Y.; Chou, Y. W.; Lin, C. J.; Zhou, Z. L.; Shiue, Y. L.; Wei, K. C.; Yang, H. W. Bioengineering Fluorescent Virus-Like Particle/RNAi Nanocomplexes Act Synergistically with Temozolomide to Eradicate Brain Tumors. *Nanoscale* **2019**, *11*, 8102−8109.

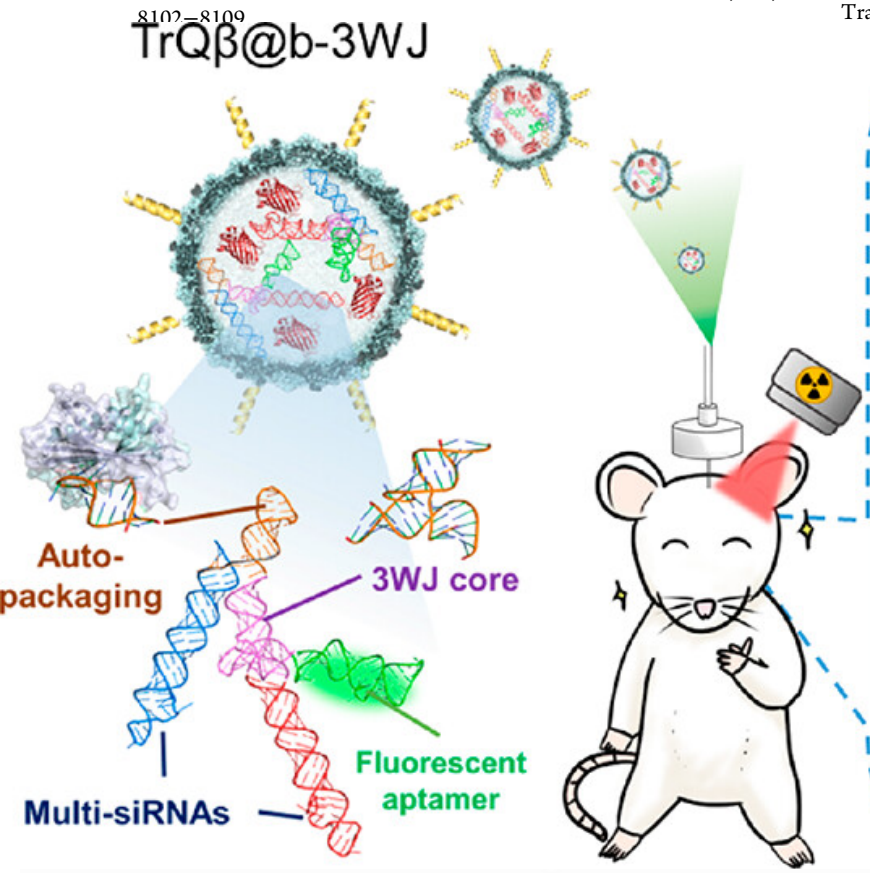

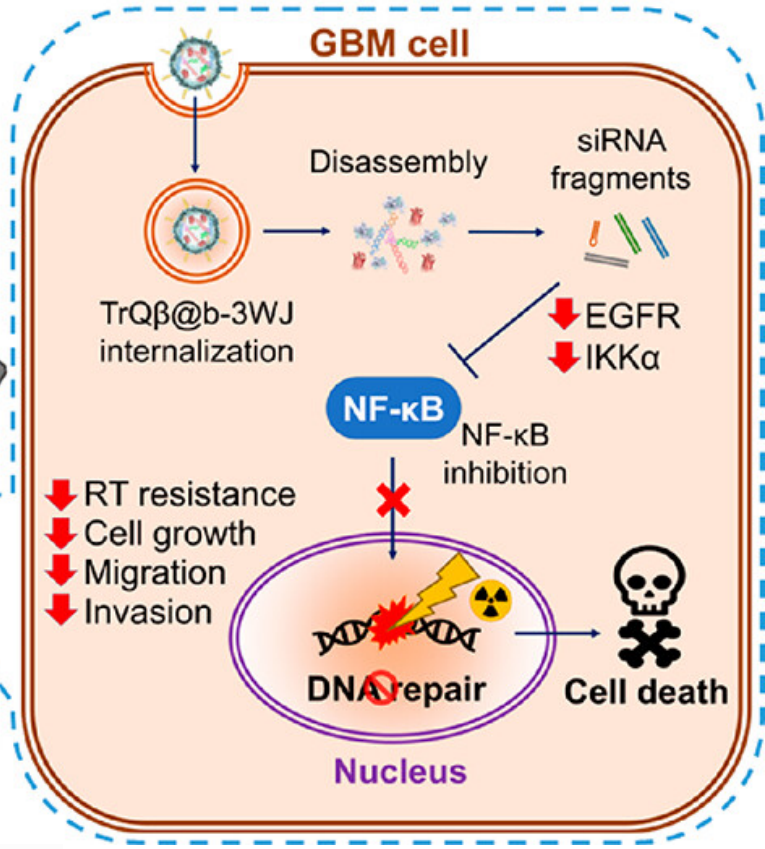

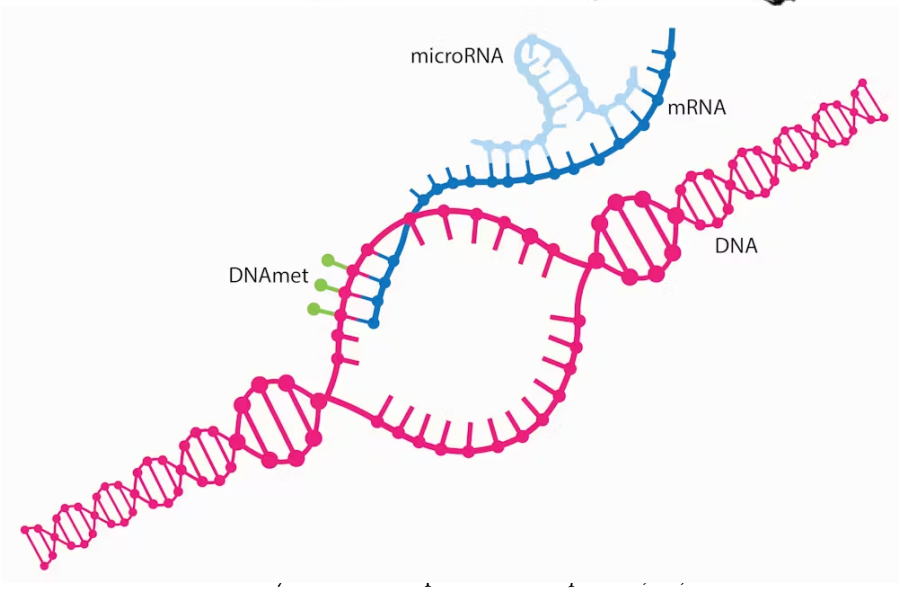

1278.
(41) Kubo, N.; Noda, S. E.; Takahashi, A.; Yoshida, Y.; Oike, T.; Murata, K.; Musha, A.; Suzuki, Y.; Ohno, T.; Takahashi, T.; et al. Radiosensitizing Effect of Carboplatin And Paclitaxel to Carbon-Ion Beam Irradiation in The Non-Small-Cell Lung Cancer Cell Line H460. *J. Radiat. Res.* **2015**, *56*, 229−238.
(42) Devereaux, Z. J.; Roy, H. A.; He, C. C.; Zhu, Y.; Cunningham, N. A.; Hamlow, L. A.; Berden, G.; Oomens, J.; Rodgers, M. T. Influence of 2′-Fluoro Modification on Glycosidic Bond Stabilities and Gas-Phase Ion Structures of Protonated Pyrimidine Nucleosides. *J. Fluor. Chem.* **2019**, *219*, 10−22.
(43) Severins, I.; Szczepaniak, M.; Joo, C. Multiplex Single-Molecule DNA Barcoding Using an Oligonucleotide Ligation Assay. *Biophys. J.* **2018**, *115*, 957−967.
(44) Liccardi, G.; Hartley, J. A.; Hochhauser, D. EGFR Nuclear Translocation Modulates DNA Repair Following Cisplatin and

https://doi.org/10.1021/acsnano.3c01102
ACS Nano 2023, 17, 10407−10422